



Spatial and temporal trends in exhumation of the Eastern Himalaya and syntaxis as determined from a multitechnique detrital thermochronological study of the Bengal Fan

Yani Najman^{1,†}, Chris Mark^{2,§}, Dan N. Barfod³, Andy Carter⁴, Randy Parrish⁵, David Chew², and Lorenzo Gemignani⁶

¹Lancaster Environment Centre, Lancaster University, Lancaster LA1 4YQ, UK

²Irish Centre for Research in Applied Geosciences, Department of Geology, Trinity College Dublin, Museum Building, College Green, Dublin 2, Ireland

³Natural Environment Research Council Argon Isotope Facility, Scottish Universities Environmental Research Centre, East Kilbride G75 0QF, UK

⁴London Geochronology Centre, Kathleen Lonsdale Building, University College London, London WC1E 6BT, UK

⁵School of Earth and Environmental Sciences, Portsmouth University, Portsmouth PO1 3QL, UK

⁶Department of Earth Sciences, Vrije Universiteit, 1081 Amsterdam, Netherlands

ABSTRACT

The Bengal Fan provides a Neogene record of Eastern and Central Himalaya exhumation. We provide the first detrital thermochronological study (apatite and rutile U-Pb, mica Ar-Ar, zircon fission track) of sediment samples collected during International Ocean Discovery Program (IODP) Expedition 354 to the mid-Bengal Fan. Our data from rutile and zircon fission-track thermochronometry show a shift in lag times over the interval 5.59–3.47 Ma. The oldest sample with a lag time of <1 m.y. has a depositional age between 3.76 and 3.47 Ma, and these short lag times continue to be recorded upward in the core to the youngest sediments analyzed, deposited at <1 Ma. We interpret the earliest record of short lag times to represent the onset of extremely rapid exhumation of the Eastern Himalayan syntaxial massif, defined as the syntaxial region north of the Nam La Thrust. Below the interval characterized by short lag times, the youngest sample analyzed with long lag times (>6 m.y.) has a depositional age of 5.59–4.50 Ma, and the zircon and rutile populations then show a static peak until >12 Ma. This interval, from 5.59–4.50 Ma to >12 Ma,

is most easily interpreted as recording passive erosion of the Greater Himalaya. However, single grains with lag times of <4 m.y., but with high analytical uncertainty, are recorded over this interval. For sediments older than 10 Ma, these grains were derived from the Greater Himalaya, which was exhuming rapidly until ca. 14 Ma. In sediments younger than 10 Ma, these grains could represent slower, yet still rapid, exhumation of the syntaxial antiform to the south of the massif. Lag times <1 m.y. are again recorded from 14.5 Ma to the base of the studied section at 17 Ma, reflecting a period of Greater Himalayan rapid exhumation. Mica ⁴⁰Ar/³⁹Ar and apatite U-Pb data are not sensitive to syntaxial exhumation: We ascribe this to the paucity of white mica in syntaxial lithologies, and to high levels of common Pb, resulting in U-Pb ages associated with unacceptably high uncertainties, respectively.

INTRODUCTION

The evolution of the Himalaya is of wide geological significance: The orogen is a type example of continent-continent collision, the Himalayan syntaxes record unusually young metamorphism and rapid exhumation compared to the main part of the orogen (e.g., Burg et al., 1997), and the development of the eastern and western syntaxes has been proposed as the archetype example of tectonic-erosion coupling (e.g., Zeitler et al., 2014). However, the exhumation history of the syntaxes remains

controversial. This work focuses on the Bengal Fan system, which drains the eastern syntaxis. The timing of onset of rapid exhumation of the eastern syntaxis is proposed to be from as early as 10 Ma to possibly as late as the Pleistocene (e.g., Wang et al., 2014; Zeitler et al., 2014).

Bedrock and detrital studies provide complementary approaches to deciphering the history of an orogen, with the detrital approach allowing insight into past tectonics that may have been obscured in the mountain belt itself by later tectonism, erosion, or metamorphism. The Bengal Fan, with its catchment in the Eastern and Central Himalaya, provides the largest integrated detrital record of the Himalayas, representing a considerably greater catchment area compared to the Indus River–Indus Fan system, which drains the western side of the range. The Bengal Fan is supplied primarily by the Yarlung-Brahmaputra River system. This river system flows along the India-Asia suture zone as the Yarlung Tsangpo, crosses the Eastern Himalayan syntaxis (Namche Barwa) and Himalayan range as the Siang River, and finally emerges at the range front, from which it flows through the onshore Bengal Basin as the Brahmaputra. During the passage of the Brahmaputra through the Bengal Basin, tributaries draining the northern Indo-Burman Ranges (IBR) and the southern slopes of the Himalaya join the system, as does the Ganges, which drains the Himalayan southern slopes as well as Peninsular India to the south (Fig. 1). The advantages of studying the Bengal Fan record over Himalayan foreland basin detrital records are: (1) the wider upland

[†]Corresponding author

[§]Present address: School of Earth Sciences, University College Dublin, Science Centre West, Belfield, Dublin D04 V1W8, Ireland.

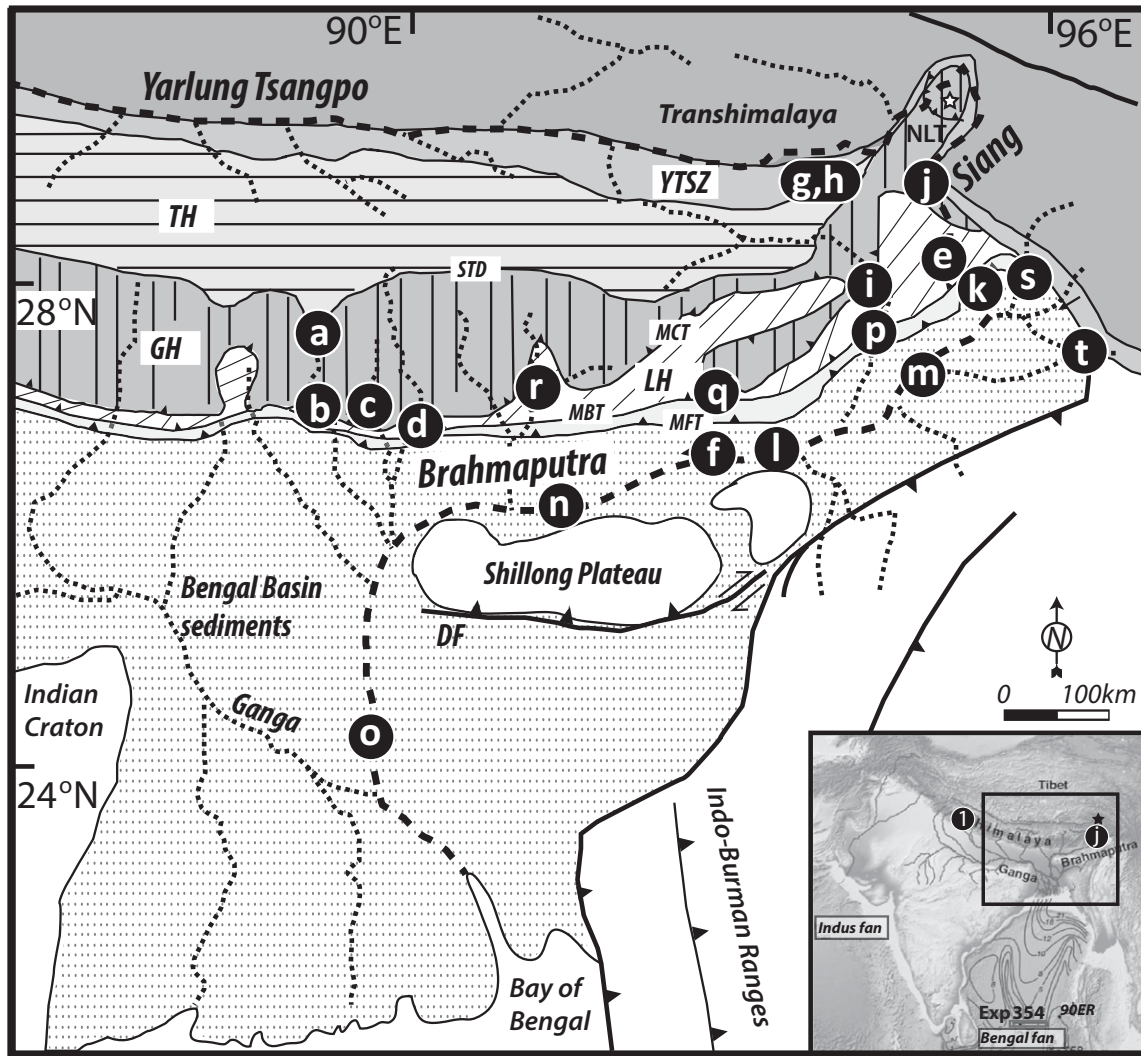


Figure 1. Map showing location of the eastern Himalayan Namche Barwa syntaxis (star), modern drainage pattern, and location of published (Bracciali et al., 2013, 2016; Gemignani, 2018; Gemignani et al., 2018) modern river sediment rutile U-Pb, mica $^{40}\text{Ar}/^{39}\text{Ar}$, and zircon fission-track (ZFT) data used to construct the basal panels of Figure 2. Sample numbers (circled) show the modern river sediments analyzed using the following approaches: (a and b) Mo Chu, rutile U-Pb; (c) Mau Khola, rutile U-Pb; (d) Mangdi Chu, rutile U-Pb; (9) Siang, rutile U-Pb; (f) Brahmaputra, rutile U-Pb; (g and h) Nanyiqu and Nanyiqu tributary, rutile U-Pb; (i) Subansiri, rutile U-Pb; (j) Siang, mica $^{40}\text{Ar}/^{39}\text{Ar}$; (k) Siang, mica $^{40}\text{Ar}/^{39}\text{Ar}$ and ZFT; (l–o) Brahmaputra, mica $^{40}\text{Ar}/^{39}\text{Ar}$ and ZFT; (p) Subansiri, mica $^{40}\text{Ar}/^{39}\text{Ar}$ and ZFT; (q) Kameng, mica $^{40}\text{Ar}/^{39}\text{Ar}$ and ZFT; (r) Manus, mica $^{40}\text{Ar}/^{39}\text{Ar}$; (s) Dibang, mica $^{40}\text{Ar}/^{39}\text{Ar}$ and ZFT; (t) Lohit, mica $^{40}\text{Ar}/^{39}\text{Ar}$. DF—Dauki Fault, YTSZ—Yarlung Tsangpo suture zone, TH—Tethyan Himalaya, GH—Greater Himalaya, LH—Lesser Himalaya, STD—South Tibetan detachment, MCT—Main Central Thrust, MBT—Main Boundary Thrust, MFT—Main Frontal Thrust, NLT—Nam La Thrust, which separates the syntaxial massif to the north (star shows location of Namche Barwa) from the syntaxial antiform to the south. Inset shows location of newly analyzed samples used for this study, from Bengal Fan International Ocean Discovery Program (IODP) Expedition 354, and the modern Siang (labeled j) and Marsyandi (labeled 1) Rivers (apatite U-Pb data only).

drainage area, which minimizes the effects of any local variation dominating a signal, and (2) the better depositional age constraints typically provided by marine versus continental facies. However, the disadvantages are that the signal of interest may be diluted downstream in

such a distal setting, fan lobe switching may result in an incomplete temporal record, and non-Himalayan material may be contributed to the system in this distal marine setting.

We provide the first detrital thermochronology study of Bengal Fan detritus from Inter-

national Ocean Discovery Program (IODP) Expedition 354. We applied U-Pb, $^{40}\text{Ar}/^{39}\text{Ar}$, and fission-track analyses to detrital rutile and apatite, white mica, and zircon, respectively, from the core material. Data Repository Item DR1¹ details the sample locations and their age

constraints. Our aims were: (1) to constrain the exhumation history of the Eastern Himalaya by determining age spectra and lag times and (2) to compare the utility of different chronometers for detrital provenance studies in a region where the modern detrital signal from the source region is well known.

GEOLOGICAL BACKGROUND

The Bay of Bengal, in which the Bengal Fan is located, is constrained to its north by the Himalayan range, to its east by the IBR, and to its west by Peninsular India. The Himalaya formed when India and Asia collided in the early Cenozoic (e.g., Hu et al., 2016). The orogen is composed of the Asian plate north of the Yarlung Tsangpo Suture Zone (YTSZ) and a southward-propagating thrust stack of the Tethyan Himalaya, Greater Himalaya, Lesser Himalaya, and Sub-Himalayan rocks of the Indian plate to the south of the suture (Fig. 1). The southern margin of the Asian plate, termed the Lhasa Block, consists predominantly of Mesozoic to Paleogene precollision arc batholiths of the Transhimalaya, as well as Precambrian and younger basement and Paleozoic–Mesozoic sedimentary rocks. South of the YTSZ, the Indian plate consists of: (1) Neoproterozoic–Eocene sedimentary and low-grade metasedimentary rocks (the Tethyan Himalaya), which were deposited on the Tethyan ocean passive margin; (2) predominantly medium- to high-grade metamorphic rocks with leucogranites (the Greater Himalaya), which were subjected to metamorphism and anatexis during the Cenozoic Himalayan orogeny; (3) Neoproterozoic–Cenozoic metamorphosed and unmetamorphosed Indian plate rocks, which comprise the Lesser Himalaya; and (4) the Sub-Himalaya, which is composed of Cenozoic foreland basin sedimentary rocks now incorporated into the orogen. These tectonic units are separated by the South Tibetan

Detachment System (STDS), the Main Central Thrust (MCT), and the Main Boundary Thrust (MBT), respectively (Hodges, 2000).

At the western and eastern terminations of the orogen, there lie the eastern (Namche Barwa) and western (Nanga Parbat) syntaxes, which spatially coincide with the range-front exits of the two major transorogenic river systems: the Indus and the Brahmaputra. The eastern syntaxis (Fig. 1) is drained by the Brahmaputra and is the syntaxis considered in this study. The eastern syntaxis consists of Greater Himalayan high-grade metamorphic rocks. It is folded into a NE–SW–trending north-plunging antiform bounded on its eastern, western, and northern margins by shear zones that originally formed the YTSZ, thus delineating the boundary between the Indian plate rocks of the syntaxis and the Asian plate Lhasa Block basement (e.g., Seward and Burg, 2008). In the terminology of Zeitler et al. (2014), a distinction is made between the Namche Barwa syntaxial massif in the northern part of the syntaxis and the syntaxial antiform in the south, with the two regions separated by the Nam La Thrust (Fig. 1).

Although the syntaxes and the main part of the orogen share a similar early Himalayan tectonometamorphic history, their evolution diverged in the late Miocene, with younger metamorphism and more extreme exhumation in the syntaxes, as detailed further below.

While the majority of sediment delivered to the Bengal Fan is delivered by the Brahmaputra from the Himalayas, contributions are also made from the IBR to the east and Peninsular India to the west. The IBR are generally considered to represent an accretionary prism at the margin of the Indian plate and Burma platelet (Maurin and Rangin, 2009). The IBR consist of Cretaceous(?) to Paleogene sedimentary rocks considered to be derived from the West Burman arc to the east and Neogene sedimentary rocks considered to be recycled Himalayan-derived detritus that was scraped off the Bengal Fan as the Indian plate subducted (Allen et al., 2008). Eastern Peninsular India consists of Proterozoic mobile belts in the north and, further south, Archaean craton.

Tectonothermal Evolution of the Eastern Himalaya and Syntaxis

Pressure-temperature-time (P - T - t) calculations indicate that the eastern syntaxis and Greater Himalayan rocks of the main part the orogen underwent a similar Paleogene and early Neogene metamorphic history, as summarized, for example, by Palin et al. (2015). Along the main part of the range, Greater Himalayan regional kyanite-grade peak metamorphic condi-

tions of 9–12 kbar and 550–680 °C were reached around 37–30 Ma, and subsequent decompression and heating resulted in sillimanite-grade metamorphism, with associated migmatization and the formation of leucogranites between ca. 24 and 15 Ma (e.g., Cottle et al., 2009; Godin et al., 2001; Searle et al., 2009; Simpson et al., 2000; Vannay and Hodges, 1996). Similar metamorphic conditions affected the rocks within the region of the syntaxis, with P - T conditions of 11–18 kbar and 750–950 °C from 42 to 30 Ma, followed by P - T conditions of 4–10 kbar and 650–900 °C between ca. 24 and 8 Ma. Recent metamorphism in the core of the syntaxis is recorded by P - T conditions of 7–8 kbar and 550–650 °C around ca. 11 to 3 Ma (e.g., Booth et al., 2009; Burg et al., 1998; Ding et al., 2001; Guilmette et al., 2011; Liu et al., 2011; Xu et al., 2010; Zeitler et al., 2014; Zhang et al., 2010).

Initiation of rapid exhumation of the Greater Himalaya was associated with movement along the MCT in the early Miocene (e.g., Hubbard and Harrison, 1989). Although there are considerable along- and across-strike variations, typical Greater Himalayan cooling rates were in the range of ~10–60 °C/m.y. and exhumation rates were in the range of ~2 mm/yr over the interval ca. 23–16 Ma (e.g., Vannay et al., 2004), decreasing thereafter. In the eastern Himalaya, rapid exhumation of the Greater Himalaya ceased around 14–13 Ma in much of the region (e.g., Godin et al., 2006; Kellett et al., 2013), with rapid exhumation then propagating into the footwall of the MCT; cooling rates over the interval ca. 11–2 Ma have been calculated at ~20–70 °C/m.y., with associated exhumation of ~1.5–3 mm/yr (e.g., Thiede and Ehlers, 2013; Vannay et al., 2004). However, in some areas, renewed ductile thrusting along the MCT zone is recorded at 10 to <8 Ma, followed by rapid exhumation (Braden et al., 2017, 2018; Catlos et al., 2004), and more widely documented exhumation of the Greater Himalaya is further recorded with exhumation rates between ~1.5 and 2.5 mm/yr after ca. 4 Ma (Thiede and Ehlers, 2013; Vannay et al., 2004).

By contrast, exhumation rates in the eastern syntaxial massif are considerably higher (e.g., Enkelmann et al., 2011) and debated. Calculations range from 5–10 mm/yr for up to the last 10 m.y. (Zeitler et al., 2014); to 10 mm/yr between 3.5 and 3 Ma (Burg et al., 1997), decreasing to a maximum of 2 mm/yr for the last 2.5 m.y. (Seward and Burg, 2008); to 4 mm/yr during the Pleistocene (Bracciali et al., 2016); to 9 mm/yr over the past 1 m.y. (King et al., 2016).

The more recent metamorphism and rapid exhumation of the syntaxis compared to the main part of the orogen are responsible for the unusually young late Pliocene to Quaternary

¹GSA Data Repository item 2019108, Item DR1: Sample list, including age constraints; Item DR2: U-Pb methods for apatite and rutile; Item DR3: U-Pb data for apatite (3a) and rutile (3b); Item DR4: Mica ⁴⁰Ar/³⁹Ar data and supplementary methods; Item DR5: Zircon fission-track data; Item DR6: Youngest-array Tera-Wasserburg plots for rutile U-Pb data; Item DR7: Figure showing kernel density estimation plots (as for Fig. 2) but for samples with depositional ages older than 10 Ma; Item DR8: Zr-in-rutile thermochronometry; Item DR9: Comparison of (A) U-content; (B) fraction (f_{206}) of total ²⁰⁶Pb that is common, i.e., nonradiogenic; (C) absolute nonradiogenic ²⁰⁶Pb in analyzed apatite and rutile; and (D) f_{206} vs. single-grain uncertainty, where n = number of analyzed grains, is available at <http://www.geosociety.org/datarepository/2019> or by request to editing@geosociety.org.

mineral cooling and (re)crystallization ages in the syntaxial massif, including zircon and apatite fission-track and (U-Th)/He, biotite and hornblende $^{40}\text{Ar}/^{39}\text{Ar}$, and zircon, rutile, titanite, xenotime, and thorite U-Pb ages (Bracciali et al., 2016; Seward and Burg, 2008; Zeitler et al., 2014). The simplest explanation for these data is that rocks presently exposed at the surface within the syntaxis resided at temperatures in part above 500 °C as recently as Pliocene times, as recorded by bedrock rutile dated at younger than 1 Ma (Bracciali et al., 2016). This feature is absent from the main part of the Himalaya orogen outside the syntaxes, where medium-temperature thermochronometer ages (e.g., white mica $^{40}\text{Ar}/^{39}\text{Ar}$, zircon fission track [ZFT], rutile U-Pb) are predominantly Miocene in age, for example, in far east Nepal (e.g., Larson et al., 2017), Sikkim (e.g., Kellett et al., 2013), Bhutan (e.g., Coutand et al., 2014), and Arunachal Pradesh (e.g., Adlakha et al., 2013; Yin et al., 2010).

The onset of the rapid syntaxial exhumation has been variously proposed at ca. 10 Ma (Zeitler et al., 2001, 2014), ca. 8 Ma (Palin et al., 2015), before 7 Ma (Govin, 2017), by ca. 7–5 Ma (Lang et al., 2016), ca. 4 Ma (Burg et al., 1998), not before 4 Ma (Chirouze et al., 2013), sometime between 7 and 3 Ma with exhumation likely predominantly a Pleistocene feature (Bracciali et al., 2016), or not until 2.5–2 Ma (Wang et al., 2014), although Zeitler et al. (2015) extrapolated a rapid exhumational onset of 4–3 Ma from the data set of Wang et al. (2014). Furthermore, variations in the locus of rapid exhumation within the syntaxial region are similarly debated. Several authors (King et al., 2016; Seward and Burg, 2008; Yang et al., 2018) have proposed migration/expansion of the locus of syntaxial exhumation toward the NE with time. In contrast, Zeitler et al. (2014) proposed that the wider syntaxial region (syntaxial antiform and massif, and the syntaxis-proximal Lhasa Block basement) began rapid exhumation around ca. 10 Ma, with this rapid exhumation ceasing in the Lhasa Block around ca. 7–6 Ma, in the antiform around ca. 4 Ma, and continuing or accelerating in the massif after that time.

The controlling mechanism for the tectonic history of the paired eastern and western syntaxes, with their similar locations and fluvial drainage, is equally poorly understood; the two end-member scenarios relate to whether the deep incision of the Brahmaputra and Indus Rivers or the unique tectonic setting in the corners of the orogen was the ultimate cause (Wang et al., 2014, 2015; Zeitler et al., 2015). Restricting this summary to the eastern syntaxis, Burg et al. (1997) proposed structural buckling within the constricted corner of the orogen migrating north

through time (Seward and Burg, 2008; Yang et al., 2018). Zeitler et al. (2001, 2014) put forward the region as a type example of tectonic-erosion coupling. In their “tectonic aneurysm” model, rapid fluvial incision by the Brahmaputra River weakened the crust, leading to advective flow of midcrustal material toward the region of the topographic gap. However, Wang et al. (2014) considered that the rapid downcutting of the Brahmaputra was the result of, rather than the cause of, syntaxial exhumation. More recently, Bendick and Ehlers (2014) suggested a model in which the rapid exhumation was the result of the subduction geometry at the indenter corners of the downgoing plate.

Detrital Record of Eastern Himalayan and Syntaxial Evolution

Due to inaccessibility of much of the region, a paucity of structural and metamorphic data from the eastern syntaxis has hindered progress in deciphering its tectonic evolution. Thus, detrital studies are particularly useful for understanding the metamorphic and exhumational history of the eastern syntaxis on a regional scale. In this study, we employed U-Pb analyses on detrital rutile and apatite, $^{40}\text{Ar}/^{39}\text{Ar}$ analyses on detrital white mica, and fission-track analyses on detrital zircon from Himalayan-derived Bengal Fan sediment. Existing data are summarized below, apart for the apatite U-Pb system, for which no published data exist for the Eastern Himalaya (but note also Govin, 2017), and only one data set is available for the western Himalaya (Turab et al., 2017); thus, we present new apatite U-Pb data we produced to characterize the source region’s characteristics in terms of the U-Pb isotopic system.

Modern River Data

Analyses from modern river sediments draining the eastern syntaxis and the Eastern Himalaya adjacent to but outside the syntaxis (Fig. 2, basal panels) are consistent with bedrock thermochronology data. Published modern river detrital rutile U-Pb, mica $^{40}\text{Ar}/^{39}\text{Ar}$, and ZFT ages from rivers draining the Eastern Himalaya outside the syntaxis are predominantly Oligocene to Miocene in age, with all rutile ages older than 9 Ma (Bracciali et al., 2013), all mica ages older than 4–3 Ma (Bracciali et al., 2016; Lang et al., 2016), with the exception of two rivers close to the syntaxis, which yielded one $^{40}\text{Ar}/^{39}\text{Ar}$ mica age of 2.24 ± 1.75 Ma and one of 0.95 ± 1.14 Ma (Gemignani et al., 2018), and all ZFT ages younger than 4 Ma (Enkelmann et al., 2011). In contrast, grains from rivers draining the syntaxis have yielded ages as young as <1 Ma for all the thermochronological systems described above

(Bracciali et al., 2016; Enkelmann et al., 2011; Gemignani et al., 2018; Lang et al., 2016). No published apatite U-Pb data exist from modern Himalayan rivers; therefore, we collected and describe our new data here (Fig. 2, basal panel). Our apatite U-Pb data show that the youngest apatite U-Pb grain age recorded from the Siang River draining the syntaxis is ca. 2 Ma, with the youngest peak at ca. 6 Ma. This is considerably younger than the ca. 28 Ma youngest peak, and ca. 15 Ma youngest grains recorded from modern river sediments draining Eastern Himalayan regions outside the syntaxis. Similarly older ages are recorded in the western Himalaya outside of the Nanga Parbat syntaxis, where all grains are older than 18 Ma (Turab et al., 2017).

Foreland Basin Data

Thermochronological ZFT and mica $^{40}\text{Ar}/^{39}\text{Ar}$ lag-time data (the difference in age between a detrital grain’s thermochronological age and the depositional age of its host strata) from foreland basin sections were summarized by Lang et al. (2016). They noted that in sedimentary sections adjacent to the main part of the orogen, lag times remain constant or increase up section, while in sedimentary sections proximal to the syntaxes, lag times decrease up section. Sedimentary sections along the main central part of the orogen in India and west and central Nepal show zero lag times and thus rapid exhumation by 21 Ma, with lag times increasing to >4–6 m.y. at 17 Ma




Figure 2. Detrital zircon fission-track (ZFT), white mica $^{40}\text{Ar}/^{39}\text{Ar}$, apatite U-Pb, and rutile U-Pb data for all samples, and sample locations within cores. Kernel density plots were generated using DensityPlotter (Vermeesch, 2012); note logarithmic *x* axes. Ages are in Ma. Paired vertical lines denote cut-off times for grains with lag times ≤ 1 m.y., incorporating deposition age uncertainty; *n*—number of acceptable analyses/total number of analyses; *n—number of rutile and apatite grains yielding lag times <1 m.y. (lag-time calculation incorporated U-Pb age uncertainty and is based on the minimum deposition age). Basal panels are compilations of published data (Bracciali et al., 2013, 2016; Gemignani, 2018; Gemignani et al., 2018), plus our new apatite U-Pb data, showing syntaxial-draining (solid line) and non-syntaxial-draining (dashed line) rivers, displayed to illustrate characteristic differences between the two regions. Sample locations are shown on Figure 1. Sediment depositional ages were taken from France-Lanord et al. (2016) and Blum et al. (2018).**

Namche Barwa exhumation as determined from the Bengal Fan detrital record

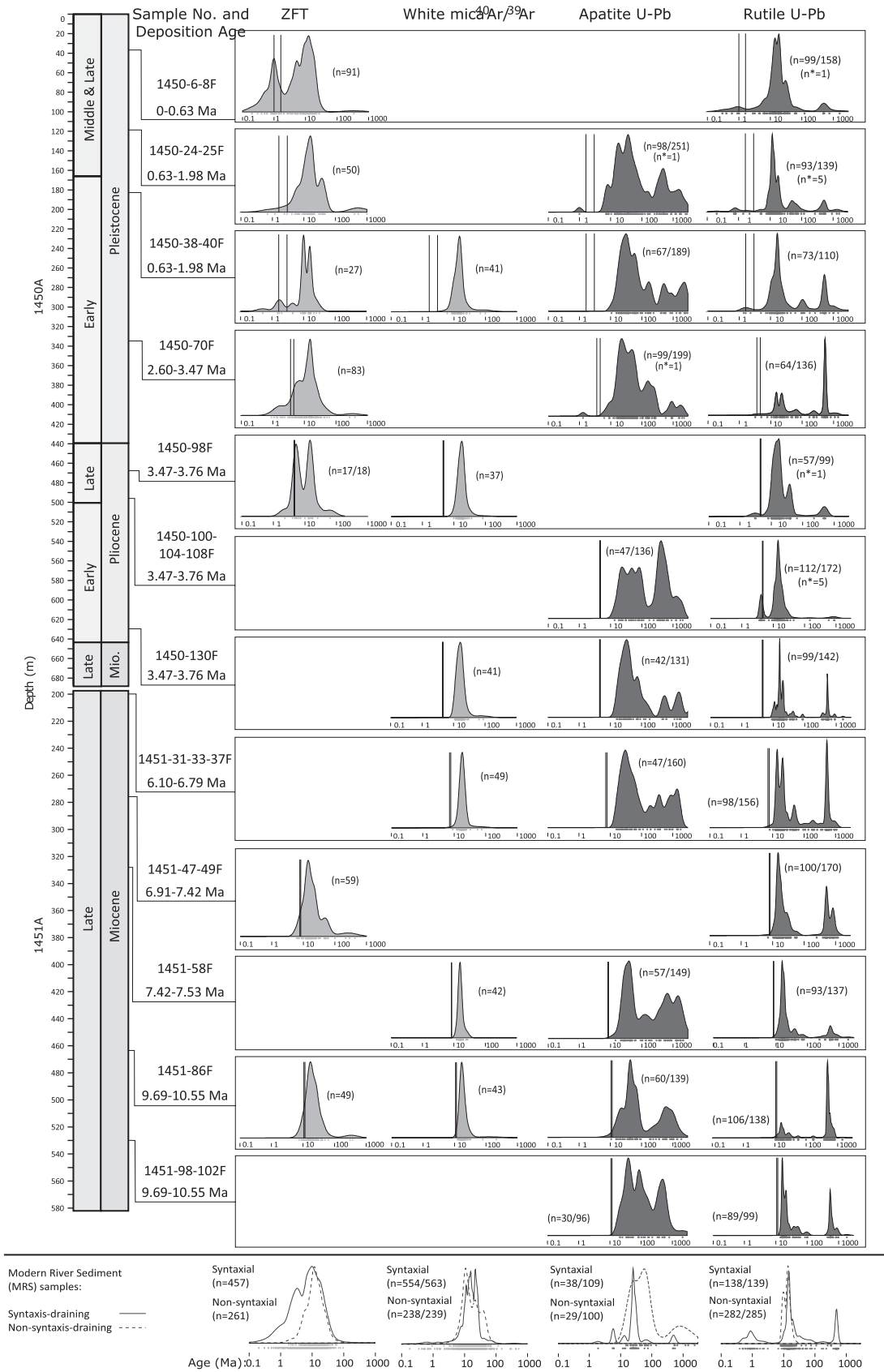


Figure 2.

in some sections and by 12–10 Ma in other sections (e.g., Bernet et al., 2006; Najman et al., 2009; Szulc et al., 2006; White et al., 2002). Similarly, in the eastern part of the orogen, sedimentary sections deposited between 13 and 7 Ma by rivers not draining the syntaxis have lag times similar (~4 m.y.) to those recorded in coeval sections in the central orogen (Chirouze et al., 2013). In contrast, foreland basin sedimentary sections that include the eastern syntaxis in their upland drainage basins show short lag times (and hence rapid exhumation) at much younger times: Lang et al. (2016) recorded short lag times (<2 m.y. for ZFT and <4 m.y. for $^{40}\text{Ar}/^{39}\text{Ar}$ micas) from 5 Ma onwards, with the work of Govin (2017) suggesting broadly similar results. However, in contrast, Chirouze et al. (2013), studying the Brahmaputra-sourced section of the Eastern Himalaya over the interval 7–3 Ma, did not detect exhumation rates higher than typical for the main central part of the orogen. Further downstream in the onshore Bengal Basin, Bracciali et al. (2016) did not record very short lag times until the deposition of the Tipam Formation between ca. 3.5 and 2 Ma, where a single rutile grain yielding a U-Pb age of 2.3 ± 1.1 Ma was documented.

Bengal Fan Data

As discussed in more detail in the section on the “Provenance of the Detrital Grains,” the Bengal Fan is considered to be predominantly derived from the Eastern Himalaya, in view of (1) the major input to the region from the Ganges-Brahmaputra, (2) the detrital zircon U-Pb signature typical of Brahmaputra input documented from the base of the fan cored in IODP Expedition 354 (Blum et al., 2018), and (3) the zero-aged lag-time signatures from detrital minerals documented in the Bengal Fan in this study and unique to the Himalayan syntaxis, as summarized in the sections “Tectonothermal Evolution of the Eastern Himalaya and Syntaxis” and “Detrital Record of Eastern Himalaya and Syntaxial Evolution.”

Earlier detrital provenance studies on the Bengal Fan have been restricted to Ocean Drilling Program (ODP) Leg 116. Copeland and Harrison (1990) used $^{40}\text{Ar}/^{39}\text{Ar}$ detrital muscovite and K-feldspar data to show that short lag times (0 m.y.) were present throughout the studied interval from 17 to 2 Ma. They also documented negative lag times (mineral ages older than the depositional age), which they ascribed to possible contamination by hydrocarbons on mass 36 in their $^{40}\text{Ar}/^{39}\text{Ar}$ analyses. They acknowledged that similar, but undetected, contamination may have affected other samples in their study. Copeland and Harrison (1990) noted the improbability of one region sustaining such

rapid exhumation over the entire period studied, without exhuming far more material than the hinterland *P-T* constraints permit (see section “Tectonothermal Evolution of the Eastern Himalaya and Syntaxis”). Thus, they suggested that pulses of rapid exhumation must have occurred in different locations in the catchment area of the Bengal Fan over time.

Apatite fission-track (AFT) analyses were also carried out on the same sample suite used by Copeland and Harrison (1990) from ODP Leg 116 by Corrigan and Crowley (1990). Corrigan and Crowley reported lag times throughout the section varying between 0 and 10 m.y., and calculated exhumation rates of ≥ 0.3 mm/yr. Both sets of authors had to amalgamate core over intervals of between 70 m and 120 m to provide enough mineral separate for analysis, which increased the uncertainties on the depositional ages and hence also the lag-time calculations.

We return to the Bengal Fan detrital record from IODP Expedition 354 (Fig. 1), which sailed in February and March 2015. Compared to Leg 116, Expedition 354 had considerably better sand-grade recovery (France-Lanord et al., 2016), in part perhaps due to better coring techniques and partly due to the more proximal nature of the drilling site. This allowed for sufficient volumes of material to be sampled for single detrital grain studies without requiring amalgamation of core intervals of potentially different age, and hence lag-time estimates are substantially improved compared to previous work because the depositional ages are better constrained. Furthermore, initial shipboard analyses from Expedition 354 suggested that the variability in sediment recorded at the location of Leg 116 (e.g., Bouquillon et al., 1990) may not be related to changes in Himalayan sources. Alternative explanations include sediment routing variability (France-Lanord et al., 2016), perhaps due to the distal nature of its location, or fan lobe switching, as, for example, recently documented by McNeill et al. (2017). Our new work, concentrating on low- to medium-temperature thermochronometers, focused on the exhumation history of the region. It complements recent geochronological work on the Bengal Fan during IODP Expedition 354 (Blum et al., 2018). That study, which undertook nearly 7000 U-Pb analyses targeting the interiors of detrital zircons from samples with depositional ages spanning ca. 17.5–0.3 Ma, documented an absence of zircons with U-Pb ages between 14 and 10 Ma. This could be interpreted as corresponding to cessation of Greater Himalayan metamorphism and anatexis, and the onset of syntaxial metamorphism, respectively; alternatively, grains younger than 10 Ma may be related to

a period of rejuvenation of the MCT zone, although only zircon rim ages, rather than core ages, recording this event have been reported thus far (Braden et al., 2017).

APPROACH AND METHODS

We provide the first multitechnique single-grain isotopic detrital study of the Bengal Fan, using methods spanning a range of temperature sensitivities, and including two recently developed techniques never before applied to Bengal Fan sediments, namely, U-Pb dating of detrital apatite and rutile. With these techniques applied to the vast catchment area of the Bengal Fan, our goals were to obtain a more representative picture of Himalayan tectonics than previously available, particularly with respect to the eastern syntaxis, as well as to evaluate the utility of different single-grain isotopic provenance techniques in this context.

Recognition of a tectonic signal in the detrital record depends on a number of factors (e.g., Malusà et al., 2016), including the fertility of the source region in terms of the minerals to be studied, the size of the source region of interest in the catchment, the erosion rates as affected by tectonic, climatic, and topographic factors, and the durability of the mineral of study during transport and burial.

Our primary objective was to document the evolution of the syntaxis, the tectonic signal of which is distinctive in view of the uniquely young and fast exhumation of this region in the Eastern Himalaya; this is readily identifiable in the sedimentary record by minerals with very young cooling ages and short lag times (see sections “Tectonothermal Evolution of the Eastern Himalaya and Syntaxis” and “Detrital Record of Eastern Himalayan and Syntaxial Evolution”). A multitechnique approach is optimal because it increases the chances of recording tectonic signals in light of the above factors, and it also allows for a range of thermochronometers that span a range of temperature sensitivities (e.g., Carrapa, 2010; O’Sullivan et al., 2016). The techniques we employed spanned a range of temperature sensitivities for typical grain sizes and cooling rates: ~250–300 °C for the ZFT system, depending on level of radiation damage (Rahn et al., 2004); ~350–400 °C for the white mica $^{40}\text{Ar}/^{39}\text{Ar}$ system (Harrison et al., 2009; McDougall and Harrison, 1999); ~375–550 °C for the apatite U-Pb system (Cochrane et al., 2014); and 490–640 °C for the rutile U-Pb system (Kooijman et al., 2010). Resetting of the U-Pb system in both rutile and apatite can also occur during metamorphism by means of neocrystallization and recrystallization of inherited grains. For rutile, this has been documented

at temperatures as low as ~430 °C by Zack et al. (2004). However, we consider this unlikely for the rutiles studied here, if the range of crystallization temperatures we report based on the Zr-in-rutile thermometer is accepted (see “Results” section). In apatite, (re)crystallization is rare at temperatures <~400 °C (Henrichs et al., 2018; Zeh, 2004), and it is frequently widespread at temperatures >500 °C, which overlap with the thermal window for effective Pb diffusion (~375–550 °C).

We chose the rutile U-Pb and ZFT systems because previous work has shown that these two systems, spanning a range of closure temperatures, both show a clear differentiation in mineral age between syntaxial- and non-syntaxial-derived grains (see “Modern River Data” section; Fig. 2, base panel) and thus will permit tracking of the evolution of the syntaxis. Inclusion of AFT analyses would extend the range of this multichronometer study to lower temperatures, thus potentially documenting rapid syntaxial exhumation even closer to its onset. However, unlike the methods listed above, AFT lag times <1 m.y. are not unique to the syntaxis; indeed, they are common in the Greater Himalaya (e.g., Burbank et al., 2003). Therefore, an independent method of assessing the syntaxial provenance of apatite grains would be required if they were to be used for documentation of syntaxial exhumation. We had hoped that apatite U-Pb dating would provide such an independent provenance constraint, since rutile U-Pb dating (a thermochronometer with only marginally higher closure temperatures compared to the apatite U-Pb system) allows easy discrimination between syntaxial and non-syntaxial sources, as described above. However, our study showed that the apatite U-Pb system proved not to be suitable to discriminate between syntaxial and non-syntaxial sources, for reasons we discuss later (see “Assessment of the Utility of a Multi-technique Approach...” section).

We chose to analyze white mica for $^{40}\text{Ar}/^{39}\text{Ar}$ dating in order to assess the conclusions regarding spatial and temporal variation of exhumation over the catchment of the Bengal Fan, as previously studied by Copeland and Harrison (1990) using the distal Bengal Fan record and this technique (“Bengal Fan Data” section). White mica $^{40}\text{Ar}/^{39}\text{Ar}$ analyses are less suitable for tracking the exhumation of the syntaxis for two reasons. First, a study of the modern Brahmaputra showed that the short lag-time signal of the syntaxis is appreciably reduced downstream (Bracciali et al., 2016; Gemignani et al., 2018), presumably due to dilution or fertility bias, since white micas are uncommon in the metamorphic facies exposed today in the eastern syntaxis. Second, new white mica $^{40}\text{Ar}/^{39}\text{Ar}$ data show

that young white mica ages are not unique to the syntaxis (Gemignani et al., 2018); rare micas from two tributaries located in the Eastern Himalaya outside the syntaxis show <1 m.y. lag times for the $^{40}\text{Ar}/^{39}\text{Ar}$ white mica system, although ZFT ages from this river retain the longer lag-time signal typical of regions outside the eastern syntaxis.

Sand samples were taken from IODP Expedition 354 (Bengal Fan) sites 1450 and 1451, located on the medial fan (Figs. 1 and 2; Data Repository Item DR1 [see footnote 1]). Sand became rare below depths corresponding to ca. 10 Ma, and thus our data are largely concentrated over the 10–0 Ma time interval, with three older samples (depositional ages spanning ca. 17–12 Ma). Fortunately, the 10–0 Ma time period encompasses the range of ages proposed for the onset of rapid syntaxial exhumation, allowing us to adequately investigate syntaxial exhumation history.

Depositional age constraints were taken from biostratigraphic data (Blum et al., 2018; France-Lanord et al., 2016). For apatite, rutile, and zircon, we aimed to analyze ~100 grains per sample where mineral abundance permitted. However, for mica analyses, we analyzed ~300 grains in total, spanning the entire depositional range of 10–0 Ma plus the older 17 Ma sample, to search for zero-age lag times as previously documented at the drill sites of Leg 112.

For most of the thermochronological techniques, the data can be compared with existing onshore data for source characterization. However, for apatite U-Pb dating, no previously published source area characterization existed for the Eastern Himalaya. We therefore also analyzed one modern river sand sample from the Siang River (sample S6), which drains the syntaxis, and one sand sample from the Marsyandi River (sample MA10), draining a region outside the syntaxis, to obtain representative apatite U-Pb ages for these two catchment regions. Both samples are shown on Figure 1 (inset).

Apatite U-Pb Geochronology

Following mineral separation using standard techniques at various laboratories involved in IODP Expedition 354, apatite grain selection, isotopic analysis, and data reduction were performed at Trinity College Dublin. A Teledyne Analyte Excite 193 nm ArF excimer laser-ablation system with a Helix 2-volume ablation cell was utilized, coupled to an Agilent 7900 quadrupole inductively coupled plasma–mass spectrometer (ICP-MS). Repeated measurements of the Madagascar apatite primary U-Pb age standard (Thomson et al., 2012) were used to correct for analytical drift, mass bias, and

downhole fractionation, while the Durango and McClure Mountain apatites were employed as secondary age standards and treated as unknowns during analysis (McDowell et al., 2005; Schoene and Bowring, 2006). Data reduction was performed using the “VizualAge_UcomPbine” data reduction scheme (DRS) for Iolite (Chew et al., 2014; Paton et al., 2011). Due to the typically high and variable common (i.e., nonradiogenic) Pb content (Pb_c), apatite analyses are normally discordant in the U-Pb isotope system. Therefore, a ^{207}Pb -based correction was employed, which utilized known initial $^{207}\text{Pb}/^{206}\text{Pb}_c$ ratios for the primary and secondary standards.

For the McClure Mountain and Durango secondary standards, mean ^{207}Pb -corrected ages of 520.3 ± 2.0 Ma and 32.0 ± 0.3 Ma were obtained, respectively (all reported mean ages for apatite and rutile standards are weighted by, and reported at, the fully propagated uncertainty at the 2σ level, here and throughout; trace-element values for rutile standards are weighted by internal analytical uncertainty at the 2σ level). The former is indistinguishable from the accepted age of 523.5 ± 2.1 Ma (McDowell et al., 2005); the latter is ~0.3% outside the 2σ uncertainty of the accepted age of 31.4 ± 0.2 Ma (Schoene and Bowring, 2006) and probably reflects the absence of a Th/U disequilibrium correction.

For the unknowns, an initial estimate of the common-Pb ratio was generated using a terrestrial Pb isotope evolution model (Stacey and Kramers, 1975), following which an iterative approach to the age calculation was adopted. Calculation of ^{207}Pb -corrected ages was carried out using the Isoplot add-in for Microsoft Excel (Ludwig, 2012), and all associated uncertainties are reported at the 2σ level and incorporated propagated analytical error. Use of a ^{207}Pb -based correction prevents data screening using traditional measures of discordance; nonetheless, the often very high common to radiogenic Pb ratio can result in ages associated with undesirably high uncertainty. Thus, we adopted a screening approach similar to that of Zattin et al. (2012) and Mark et al. (2016). Ages older than 100 Ma were permitted uncertainty of $\leq 25\%$; ages of 100–10 Ma were permitted uncertainty of $\leq 50\%$; and ages younger than 10 Ma were permitted uncertainty of ≤ 5 Ma. Full analytical methods, isotopic ratios, and ages are reported in Data Repository Items DR2 and DR3a (see footnote 1).

Rutile U-Pb Geochronology and Trace-Element Data

U-Pb analysis followed the same procedure and instrumentation as described above for apatite U-Pb analysis, including use of the

²⁰⁷Pb-based correction and the age screening approach. The primary age standard used was R10 rutile (Luvizotto et al., 2009), and the secondary standards were R19 and RZ3 rutile (Luvizotto et al., 2009; Shi et al., 2012), which were treated as unknowns during analysis and data reduction. For the R19 and RZ3 secondary standards, mean ²⁰⁷Pb-corrected ages of 489.6 ± 2.1 Ma and 1806 ± 12 Ma were obtained, respectively. The former is indistinguishable from the accepted age of 489.5 ± 0.9 Ma (Luvizotto et al., 2009); the latter is ~0.4% outside the 2σ uncertainty limit of the 1777 ± 10 Ma age originally reported by Shi et al. (2012), but it is indistinguishable from the revised age of 1781 ± 15 Ma (Xia et al., 2013).

In addition to the standard isotopes necessary for U-Pb geochronology, Ti (assumed to be stoichiometric in rutile) and the trace element Zr were also monitored during the same analytical sessions, both to permit Zr-in-rutile thermometry and to screen for zircon inclusions. Calculation of trace-element concentrations was performed using the "Trace Elements" DRS for Iolite (Paton et al., 2011), which implements the approach of Woodhead et al. (2007). The NIST612 synthetic reference glass was used as the primary standard, and the R10, R19, and RZ3 rutiles (Luvizotto et al., 2009; Shi et al., 2012) were employed as secondary trace-element standards and processed as unknowns. Temperature calculations for Zr-in-rutile thermometry utilized the equation of Tomkins et al. (2007) for the α -quartz field and assumed a source rock pressure of 10 kbar. Mean crystallization temperatures of 728 ± 10 °C, 647 ± 5 °C, and 659 ± 47 °C were obtained for R10, R19, and RZ3, respectively; values for R10 and RZ3 were indistinguishable from the accepted values of 731 ± 1 °C and 656 ± 20 °C, while the measured value of R19 was ~0.8% higher than the accepted value of 635 ± 2 °C. Full analytical methods, isotopic ratios, ages, and elemental abundances are reported in Data Repository Items DR2 and DR3b (see footnote 1).

White Mica ⁴⁰Ar/³⁹Ar Thermochronology

Following standard mineral separation, micas from each sample and neutron flux monitors were packaged in copper foil and stacked in quartz tubes with the relative positions of packets precisely measured for later reconstruction of neutron flux gradients. The sample package was irradiated in the Oregon State University reactor, Cd-shielded facility. Fish Canyon sanidine (28.294 ± 0.036 [1σ] Ma; Renne et al., 2011) was used to monitor ³⁹Ar production and establish neutron flux values (J) for the samples.

Between 33 and 49 single mica grains were analyzed per sample at Scottish Universities Environmental Research Centre (SUERC), East Kilbride, Scotland. The samples were housed in a doubly pumped ZnS-window laser cell, and individual sample grains were loaded into a stainless-steel planchette containing 208 circular 2 mm wells. Prior to analysis, the laser cell was baked out for 48 h at ~110 °C under ultrahigh-vacuum conditions. Gas was extracted from single crystal samples in a single fusion step using a mid-infrared (10.6 μ m) CO₂ laser with a non-Gaussian, uniform energy profile and a 2.0 mm beam diameter. Liberated argon was purified of active gases, e.g., CO₂, H₂O, H₂, N₂, and CH₄, using two Zr-Al getters, one at 16 °C and another at 400 °C. Data were collected on a Mass Analyzer Products MAP-215–50 single-collector mass spectrometer using an electron multiplier collector in dynamic collection (peak-hopping) mode.

Time-intensity data were regressed to inlet time with second-order polynomial fits to the data. The average total system blank for laser extractions, measured between each sample run, was $1.4 \pm 0.3 \times 10^{-15}$ mol ⁴⁰Ar, $3.1 \pm 1.6 \times 10^{-17}$ mol ³⁹Ar, and $18.0 \pm 5.9 \times 10^{-18}$ mol ³⁶Ar. Mass discrimination was monitored on a daily basis, between and within sample runs, by analysis of an air standard aliquot delivered by an automated pipette system (see raw data for D values applied to individual steps). All blank, interference, and mass discrimination calculations were performed with the MassSpec software package (MassSpec, version 8.16, authored by Al Deino, Berkeley Geochronology Center). Additional methodology is provided in Data Repository Item DR4 (see footnote 1).

Zircon Fission-Track Thermochronology

Multiple (≥ 3) etched Teflon grain mounts were packed with mica external detectors and Corning (CN2) dosimeter glasses and irradiated in the FRM 11 thermal neutron facility at the University of Munich in Germany. Following irradiation, the external detectors were etched using 48% HF at 20 °C for 25 min. Sample ages were determined using the zeta calibration method and International Union of Geological Sciences (IUGS) recommended age standards (Hurford, 1990). Track counting at the London Geochronology Centre, University College London, UK, used a Zeiss Axioplan microscope with a total magnification of 1250 \times . The number of zircon grains analyzed in each sample varied according to zircon abundance, quality (zoning), and age/uranium concentration (uncountable track densities). Where relatively few zircons could be analyzed (e.g., samples 1450-98F

and 1450-40F), the mixed population of zircon ages (shown as kernel density estimation plots on Fig. 2) should be treated as indicative only. The youngest population of ages (Fig. 3) was obtained using the three-parameter algorithm of Galbraith (2005), implemented in DensityPlotter (Vermeesch, 2012).

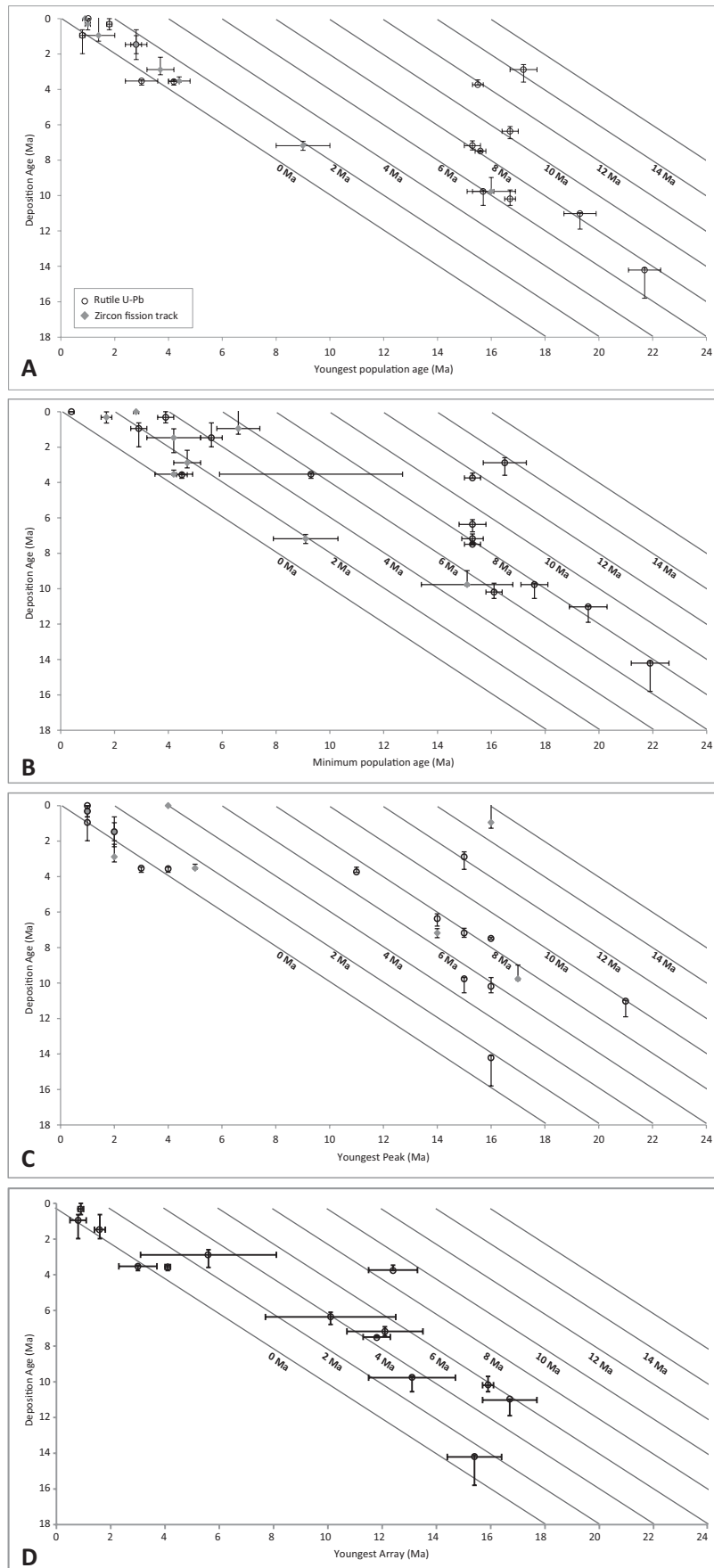
RESULTS

All data for apatite and rutile U-Pb, ⁴⁰Ar/³⁹Ar mica, and ZFT ages are summarized below and provided in full in Data Repository Items DR3, DR4, and DR5, respectively.

Data for samples encompassing the depositional period ca. 10–0 Ma are displayed in Figure 2, with the cutoff limits for 1 m.y. lag times indicated for each sample (i.e., the minimum and maximum deposition age limit for each sample plus 1 m.y.). In all plots, grains to the left (i.e., younger) of these cutoffs have lag times <1 m.y., and analyses to the right (i.e., older) have lag times >1 m.y. Rutile lag times <1 m.y. are first recorded over the interval 3.76–3.47 Ma (sample 1450-100-104-108) and from then until present day. All older samples (i.e., from sample 1450-130F, with depositional ages of 5.59–4.50 Ma and further down-core) have lag times ≥ 1 m.y., with the exception of a single grain in a sample deposited between 7.42 and 6.91 Ma, which yielded an age of 7.1 ± 4.3 Ma. As the kernel density plots displayed in Figure 2 do not incorporate uncertainty, we also report the number of rutile (and apatite) grains in each sample that have lag times <1 m.y. when U-Pb age uncertainty is also taken into account, based on minimum constraints for deposition ages.

For the other proxies, all ZFT data sets yielded some grains with lag times <1 m.y., with the proportion of <1 m.y. lag-time grains increasing in samples deposited after 3.76 Ma; no mica ⁴⁰Ar/³⁹Ar data set yielded grains with lag times <1 m.y.; and only two apatite U-Pb data sets yielded grains with lag times of <1 m.y., deposited at ca. 3 Ma and ca. 1.3 Ma.

Figure 3 clearly shows the significant shift in lag times over the interval 3.76–3.47 Ma to 5.59–4.50 Ma in the rutile and ZFT data. This shift is observed regardless of whether lag times were calculated using (A) the youngest population, obtained using the deconvolution algorithm of Galbraith (2005) implemented in DensityPlotter (Vermeesch, 2012); (B) the minimum population, obtained using the three-parameter algorithm of Galbraith (2005) implemented in DensityPlotter (Vermeesch, 2012); or (C) the youngest visually determined modal peak. As these approaches do not take into account analytical age uncertainty, we also calculated lower-intercept array ages for the rutile



U-Pb data, for which analyses yielding acceptable ages indistinguishable at the 2σ level from the age of the youngest acceptable analysis were used (D; see Data Repository Item DR6 [footnote 1]). The lag-time shift between 3.76–3.47 Ma and 5.59–4.50 Ma was also observed using this approach.

The shift between 3.76–3.47 Ma and 5.59–4.50 Ma is recorded much more subtly by the apatite U-Pb data. Figure 2 shows that for samples broadly equivalent in age to those having <1 m.y. rutile lag times, the youngest apatite U-Pb peak in all but one sample is ≤ 23 Ma, with a youngest peak in one sample of 8 Ma, and youngest single-grain ages in two samples yielding lag times <1 m.y. By contrast, for older samples, broadly equivalent to samples that have rutile lag times of >1 m.y., the youngest apatite U-Pb peaks are consistently ≥ 30 Ma, except for one sample that has a youngest peak of ca. 23 Ma.

The youngest peak in the mica $^{40}\text{Ar}/^{39}\text{Ar}$ age data varied between 18 and 15 Ma over the time interval 10–1 Ma and showed no systematic change up section, although this may be due to the relatively low grain numbers analyzed per sample (Fig. 2). Out of the 286 white mica grains analyzed in total, no grains had lag times <1 m.y. Two samples had shortest lag times of ~2.5 m.y. (as determined from the youngest grain rather than youngest peak), while all other samples had shortest lag times as determined by the youngest grain of ~5 m.y.

Figure 3. Lag times for rutile U-Pb and zircon fission-track (ZFT) data, generated using: (A) the youngest population produced by the normal mixture deconvolution algorithm of Galbraith (2005), implemented in “auto” mode in DensityPlotter (Vermeesch, 2012); (B) the minimum population calculated by the three-parameter algorithm of Galbraith (2005), implemented in DensityPlotter (Vermeesch, 2012); (C) the youngest modal peak, visually determined from the kernel density plots in Figure 2 (minimum number of grains to define a peak = 2); and (D) lower-intercept ages of the youngest array for each sample, calculated using Isoplot (Ludwig, 2012); youngest array analyses were identified as those indistinguishable at 2σ level from the youngest acceptable single-grain age in each sample (see Data Repository Item DR6 [text footnote 1]). Data at $t = 0$ (A–C only) were calculated using modern river sediment (MRS) samples, from the sources referenced in Figure 2.

Additionally, we analyzed one older sample (depositional age ca. 16.9 Ma) for white mica ($^{40}\text{Ar}/^{39}\text{Ar}$ and apatite U-Pb only) and two older samples (depositional ages ca. 12 Ma and 14.5 Ma) for rutile only (Data Repository Item DR7 [see footnote 1]). The white mica $^{40}\text{Ar}/^{39}\text{Ar}$ data showed a dominant peak of similar age to that recorded in samples younger than 10 Ma and therefore included analyses with <1 m.y. lag time at this older depositional age. Rutile data also showed this same period of short lag time in the sample dated 14.5 Ma, but not in the sample with a 12 Ma depositional age. In contrast, the apatite U-Pb data do not approach <1 m.y. lag times (youngest acceptable age 29.0 ± 2.3 Ma), and the oldest peak is of similar age to that in samples deposited between 10 and 4 Ma. For the two samples we analyzed for rutile U-Pb ages, lag times of <1 m.y. were recorded in the sample with a depositional age of ca. 14.5 Ma, but not in the sample deposited at ca. 12 Ma.

As unroofing of the syntaxis is anticipated to have involved exhumation of deeper (and therefore hotter) metamorphic rocks as exhumation progressed, crystallization temperatures for rutile of likely syntaxial origin, obtained using Zr-in-rutile thermometry, were examined to determine whether crystallization temperatures increased in more-recently deposited samples. To determine whether observed temperatures could be distinguished from temperatures recorded elsewhere in the Himalaya, crystallization temperatures were calculated for all rutile yielding U-Pb ages younger than 52 Ma. The chosen cut-off age reflects a conservative date with respect to the commonly quoted time of India-Asia collision at ca. 59–54 Ma (Hu et al., 2016; Najman et al., 2017); metamorphism arising as a result of the Himalayan orogen *sensu stricto* must therefore be younger than this age. For rutile grains yielding Himalayan (i.e., postcollisional) U-Pb ages, median crystallization temperatures as determined by the Zr-in-rutile thermometer (Tomkins et al., 2007) do exhibit a minor up-section increase from ~650–670 °C in samples deposited at ca. 10–9 Ma to ca. 687–702 °C in samples deposited at <1 Ma. In samples deposited over and since the time interval when <1 m.y. lag times are documented, the median crystallization temperatures of rutile grains with very young lag times (<1 m.y.) are higher, ranging from ~698 to ~784 °C, and also increase up section (Data Repository Item DR8 [see footnote 1]). However, observed temperatures from all samples overlap at 1σ . In addition, these values do not incorporate the known dependence of the Zr-in-rutile thermometer on both pressure and Si activity. For rocks that crystallize quartz at typical crustal pressures (e.g., 3–14 kbar cor-

responding to ~10–50 km depths at lithostatic conditions), the effect of pressure dependence on this geothermometer will be of the order ~40–75 °C; for Si-undersaturated rocks, such compositional effects should not exceed ~60–70 °C (Meinhold, 2010; Ferry and Watson, 2007; Tomkins et al., 2007).

DISCUSSION

Provenance of the Detrital Grains

The Bengal Fan is fed predominantly from the Brahmaputra-Ganges system. Therefore, the bulk of material delivered to the fan is derived from the Himalayan orogen, with some input from Peninsular India and the IBR (Fig. 1). While channel avulsion and fan lobe switching have been recorded in the Bengal Fan (France-Lanord et al., 2016; McNeill et al., 2017), we are confident that our data set captured a broadly continuous record of erosion from the Brahmaputra-Ganges system, because: (1) the biostratigraphy indicates effectively continuous deposition (Blum et al., 2018; France-Lanord et al., 2016), and (2) U-Pb dating shows a significant presence of Mesozoic–Paleogene zircons in the Bengal Fan throughout the interval of interest (Blum et al., 2018). Grains of such age are characteristic of the Transhimalaya, along which the upper reaches of the Yarlung-Brahmaputra River flows. Although some zircons with such age ranges will undoubtedly have been derived from rocks of the Paleogene (Allen et al., 2008) or Neogene (Najman et al., 2012) IBR Burman margin to the east, the appreciable proportion of the age spectra constituting this population in the Bengal Fan indicates contribution from the Yarlung-Brahmaputra.

In the sections below, we discuss our mineral ages and lag-time data both in the light of onset of syntaxial exhumation and exhumation of the orogen on a broader spatial scale. Regarding the syntaxial exhumation, we are confident that the short lag times we record in sediments from ca. 5.59–3.47 Ma onwards are from the Himalayan syntaxis, since we are unaware of any other region in the Bengal Fan catchment that would produce similarly young grains. Lag-time data for the Himalayan orogen was summarized in the section on the “Detrital Record of Eastern Himalayan and Syntaxial Evolution” earlier herein; the western slopes of the IBR consist of recycled Himalayan-derived detritus (Allen et al., 2008), and grain ages are overwhelmingly not younger than 10 Ma for rutile U-Pb (Bracciali et al., 2015), ZFT, and mica $^{40}\text{Ar}/^{39}\text{Ar}$ (Allen et al., 2008; Najman et al., 2012). Peninsular India produces overwhelmingly old mineral grain ages (e.g., Najman et al., 2008).

More broadly, we note the dominant rutile, white mica, and ZFT age peak is ca. 15–16 Ma. This mineral population is in all probability predominantly derived from the Greater Himalaya, either transported directly, or recycled via the sedimentary rocks of the suture zone (e.g. Leary et al. 2016) or IBR (Allen et al., 2008; Najman et al. 2012). This time reflects a known period of exhumation throughout much of the orogen, from the Greater Himalaya (see section “Tectonothermal Evolution of the Eastern Himalayan and Syntaxis”) to north of the suture zone (e.g. Carrapa et al., 2014; Tremblay et al., 2015). We interpret our grains as predominantly Greater Himalayan-derived detritus in view of the paucity of rutile and white mica in the Transhimalaya; however, zircons with Neogene FT ages may be Transhimalayan-derived detritus, either derived directly, or recycled via the suture zone sedimentary rocks (e.g. Ge et al 2018).

Onset of Eastern Syntaxial Rapid Exhumation

Due to its extreme exhumation rate (see “Tectonothermal Evolution of the Eastern Himalaya and Syntaxis” section), the eastern syntaxial massif contributes perhaps as much as 70% of the modern Brahmaputra sediment load (Enkelmann et al., 2011). In the past, this contribution may have been considerably less during the early onset of the syntaxial exhumation. Nevertheless, due to the uniquely young signatures of the syntaxial massif-derived rutiles and zircons (“Tectonothermal Evolution of the Eastern Himalaya and Syntaxis” and “Detrital Record of Eastern Himalayan and Syntaxial Evolution” sections; Fig. 2, base panels), it is possible to identify syntaxial-derived grains and thus track syntaxial evolution, even for periods when this region may not have been contributing the bulk of the detritus. It should be noted, however, that further back in time, when syntaxial exhumation may have been slower, dilution of the signal would have been greater. This, plus the fact that the duration between the onset of enhanced exhumation and capture of short lag times in the sediment record is dependent on the exhumation rate during this early phase of increase, plus potential sediment storage, means that longer lag times need not represent slower exhumation, and this in turn means that our determination of the onset of rapid exhumation from the earliest recording of short lag times should be considered a minimum age.

With the above caveats in mind, the clear change to lag times of <1 m.y. in the Bengal Fan record some time over the interval 3.47–5.59 Ma indicates onset of extremely rapid syntaxial exhumation by this time (Figs. 3A and

3B). This is in excellent agreement with the 4.0–3.5 Ma age of onset of rapid exhumation associated with fold amplification documented by Burg et al. (1997, 1998), and with the data of Wang et al. (2014), which were extrapolated by Zeitler et al. (2015) to show onset of syntaxial massif evolution at 4–3 Ma. This event and the orogen-wide event relating to exhumation of the Greater Himalaya along the MCT in the early Miocene (“Tectonothermal Evolution of the Eastern Himalaya and Syntaxis” section) are clearly picked out as the two main peaks (and thus metamorphic events) in the rutile data (Fig. 4); this attests to the significance of these events in Himalayan evolution.

These data are largely at odds with equivalent data from the onshore Bengal Basin, where the coeval Tipam Formation (depositional age 3.5–2.0 Ma), interpreted as paleo-Brahmaputra deposits by Bracciali et al. (2015), contained only one rutile grain with a short lag time, in the stratigraphically highest sample (Bracciali et al., 2016). The lack of such grains in the Tipam Formation could be due to either (1) the Tipam Formation not representing paleo-Brahmaputra deposits as proposed by those authors, and instead perhaps representing sediments derived from recycling of the older paleo-Brahmaputra deposits of the Surma Group during uplift of the Shillong Plateau (Johnson and Alam, 1991), or (2) the improbability of sampling syntaxial rutile grains given that only 30–50 grains were successfully dated in each Tipam Formation sample, whereas syntaxial grains are likely to comprise no more than a few percent of the total rutile grains in the overall detritus. The first proposed scenario is inconsistent with other evidence indicating that the Tipam Formation is not recycled from the underlying Surma Group sediments, namely, the increase in both grain size (Najman et al., 2016) and in the proportion of arc-derived material in the Tipam Formation compared to the underlying Surma Group. The increase in arc-derived material also mirrors the increase recently recorded in the Bengal Fan (Blum et al., 2018). However, while the second scenario adequately explains the paucity of rutile with short lag time in the Tipam Formation, this explanation fails to explain the corresponding lack of ZFT ages with short lag time, since such grains are common in the coeval Bengal Fan sample.

Studies that hypothesize extremely rapid syntaxial exhumation stretching back to 10 Ma (Zeitler et al., 2014) are not supported by our data; persistent <1 m.y. lag times are not reported from samples older than the time interval 3.76–3.47 Ma until their recurrence at ca. 14.5 Ma (with the latter related not to syntaxial exhumation but to rapid exhumation of the main part

of the orogen at that time; see “Tectonothermal Evolution of the Eastern Himalaya and Syntaxis” section). Nevertheless, our data over the 10–5 Ma period are equivocal. From Figures 3A–3D, we note a static peak (i.e., no change in peak age up-section) from the rutile data,

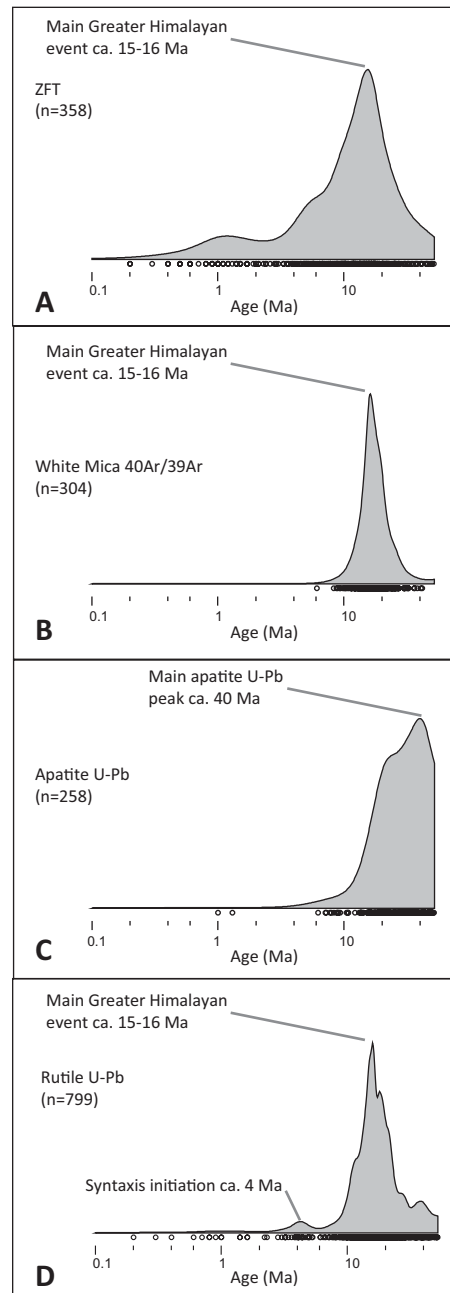


Figure 4. All acceptable Bengal Fan proxy data yielding Himalayan (younger than 52 Ma) U-Pb ages displayed as a kernel density estimation, generated using Density-Plotter (Vermeesch, 2012): (A) zircon fission track (ZFT); (B) white mica $^{40}\text{Ar}/^{39}\text{Ar}$; (C) apatite U-Pb; (D) rutile U-Pb.

most readily interpreted as passive erosion from the Greater Himalaya. However, there are rare grains with <4 m.y. lag times that persist throughout the section, even when taking into account the high analytical uncertainties. Lag times <4 m.y. would be expected in samples as young as 10 Ma, resulting from the rapid exhumation of the main part of the orogen ca. 14 Ma (see “Tectonothermal Evolution of the Eastern Himalaya and Syntaxis” section and our new rutile data). However, <4 m.y. lag times in sediments younger than 10 Ma are largely unknown in the main part of the orogen. Whether single-grain data should be given much credence is a subject of ongoing debate. If it is considered robust in this case, then this record may be tied to exhumation of the syntaxial antiform, south of the Nam La Thrust, which was exhuming at moderately rapid rates over the period 10–5 Ma (Palin et al., 2015; Zeitler et al., 2014). However, it could be difficult to distinguish this event from coeval tectonism occurring outside the syntaxial area, since a number of data sets from the MCT shear zone and Upper Lesser Himalaya in the Eastern Himalaya indicate that sufficiently high grades of metamorphism and MCT shear zone thrusting continued to ca. 10 Ma or younger, with later doming of the thrust after motion ceased (Anczkiewicz et al., 2014; Bollinger and Janots, 2006; Braden et al., 2018; Mottram et al., 2014). In fact, it is possible that the tectonometamorphic history recorded in the syntaxial anticline and that recorded in the Eastern Himalayan regions outside the syntaxis represent the same event, since rutiles of the same ca. 10 Ma age are found in Bhutan (Bracciali et al., 2013) and along strike at the southernmost part of the syntaxial antiform (Bracciali et al., 2016), and both regions show younger mineral ages to the north (Mottram et al., 2015; Zeitler et al., 2014).

In summary, our data record extremely rapid exhumation of the syntaxial massif in the Bengal Fan detrital record between the intervals 5.59–4.50 Ma and 3.76–3.47 Ma, as evidenced by first appearance, in the younger interval, of lag times of <1 m.y. in the rutile and ZFT thermochronometers. Overall, assuming that sediment storage did not extend for millions of years, it is clear that our documentation of rapid exhumation starting sometime between 5.59 Ma and 3.47 Ma is not compatible with models that explain syntaxial evolution either by river capture (Zeitler et al., 2001), which occurred in the early Miocene (Bracciali et al., 2015), or subduction geometry at indenter corners (Bendick and Ehlers, 2014), which also would require an earlier onset. Our data set is compatible with models that explain syntaxis formation as a result of crustal buckling of the constricted corner

of the orogen beginning at ca. 3.5 Ma (Burg et al., 1997; Burg and Schmalholz, 2008), but the trigger for crustal buckling at this time remains unclear.

Lag times of <4 m.y. are recorded to the base of the studied section, but it is not clear whether those recorded in sediments younger than 10 Ma relate to exhumation of the syntaxial antiform south of the massif or to the wider orogenic belt.

Spatial and Temporal Variations in Exhumation

Syntaxially derived rutile U-Pb and ZFT ages continue to record zero lag times from the interval 3.76–3.47 Ma to the present day; rutile and other mineral thermochronometers eroded from the syntaxis in the modern day yield ages younger than ca. 0.7 Ma (Bracciali et al., 2016). The production of such very short lag times for higher-temperature thermochronometers like rutile requires bringing rocks residing at >500 °C from depth to the surface within ~1 m.y., assuming that rutile U-Pb ages are dominantly controlled by thermally activated volume diffusion. Continued rapid exhumation for several million years is challenging to explain without excessive erosion to >>30 km while maintaining consistency with observed *P-T* data: Sustained rutile lag times of 1 m.y. would seem to require bringing rocks from considerable depth (10 km if the gradient was ~50 °C/km) to the surface within 1 m.y., suggesting a rate of ~10 km/m.y. and continuing this for >4 m.y.; however, such rates cannot be sustained in a given place without exhuming far more material than *P-T* data permit (i.e., a maximum of perhaps 35 km depth, or ~10 kbar pressure) as summarized in Palin et al. (2015) and the “Tectonothermal Evolution of the Eastern Himalaya and Syntaxis” section above.

There are four possible ways to reconcile this issue:

(1) The upper crust could be heated by shallow emplacement of leucogranitic rocks. This would raise the geotherm significantly, allowing a more limited amount of exhumation to explain sustained short lag times for rutile. However, sufficient volumes of leucogranites consistent with this scenario have not been recognized within the syntaxis.

(2) High exhumation rates for a shorter period of time (up to 3–4 m.y.) could be invoked at any particular locality within the syntaxis, with the locus of exhumation migrating with time. This scenario is consistent with existing *P-T-t* constraints and the lack of evidence for emplacement of significant leucogranite bodies within the syntaxis. Northward propagation of the region of highest exhumation has previously been

proposed by Seward and Burg (2008), King et al. (2016), and Yang et al. (2018).

(3) Short lag times that appear more or less constant have been explained by initial very rapid exhumation followed by a slowing of exhumation toward the present, although it may be necessary to invoke exhumation rates >10 km/m.y. for the initial period prior to the decrease in exhumation rate. In the modeling by Bracciali et al. (2016), rapid exhumation followed by slower exhumation produced steady lag times for thermochronometers, giving the impression of a “steady state.” The reason for this apparent contradiction was that in that model, as exhumation proceeds, the base of the model is brought up to the surface, so that for similar heat-flow values, the geothermal gradient continually increases.

(4) Rapid exhumation is sustained, rather than decreasing, as proposed in scenario 3 above. A thermal model with a fixed base will predict that lag times will remain constant for a constant exhumation rate, after a transient phase of a few million years. In this case, sustained exhumation of high-grade rocks >500 °C can be compatible with the total amount of exhumation calculated by invoking a combination of lateral flow from the deeper crust at amphibolite-facies conditions and then movement of this material upward into the syntaxis, where it is subjected to removal by erosional ± tectonic exhumation (Whipp et al., 2014). This scenario is consistent with *P-T* estimates while maintaining sustained high erosion rates at the syntaxis. Such a scenario was modeled by Govin et al. (2017) and Govin (2017).

In addition to the <1 m.y. lag times recognized in sediments from 3.76 to 3.47 Ma and younger, short lag times are again recorded in sediments dated at 14.5 Ma (rutile analyses) and at 16.9 Ma using white mica. This older period of rapid exhumation fits well with bedrock data, which record a period of rapid exhumation of the Greater Himalaya in the main part of the Himalaya until ca. 14 Ma (section “Tectonothermal Evolution of the Eastern Himalaya and Syntaxis”). Apart from this oldest sample, no mica grains yielded lag times approaching zero. Our data for the younger than 10 Ma interval are therefore at variance with the data from ODP Site 116 from the distal Bengal Fan (Copeland and Harrison, 1990). Contrary to the data from the distal Bengal Fan, we did not record short lag times throughout the studied interval in the Bengal Fan, and thus continuous rapid exhumation shifting to different parts of the orogen through time does not need to be invoked. The difference between the data from Site 116 and the current study could conceivably be due to the distal versus medial locations of the two study sites on the Bengal Fan. However, we consider that the most

likely cause of the difference between the two sites was the necessity for amalgamation of core material over large intervals at site 116 to allow sufficient material for analysis, which resulted in the negative lag times recorded in the Site 116 study (see “Bengal Fan Data” section) coupled with the low age resolution of those samples.

Assessment of the Utility of a Multitechnique Approach to the Application of Detrital Thermochronology to Documentation of Hinterland Tectonics

From the data set reported in this study, it is evident that the short lag times yielded by the rutile U-Pb and ZFT systems track the rapid exhumation of the syntaxis very well. However, the mica ⁴⁰Ar/³⁹Ar and apatite U-Pb systems do not.

For both the white mica ⁴⁰Ar/³⁹Ar and apatite U-Pb data: (1) there is a difference in grain ages between modern sediments from rivers draining the syntaxis and those draining regions outside the syntaxis (for the only data set from the Western Himalaya, see Turab et al., 2017). For both micas and apatites, the youngest peak is younger in rivers draining the syntaxis, and there are uncommon grains with very short lag times. (2) In the Bengal Fan, very short lag times are not recorded by either system. However, the apatite data record a subtle change at 4 Ma when the youngest peak shifts from ≥30 Ma to ≤23 Ma after this time, with a sporadic occurrence of grains ≤10 Ma.

For the white mica data, this paucity of grains with short lag times in both the modern sediment and Bengal Fan record most likely reflects the paucity of white-mica-bearing lithologies in the largely very-high-amphibolite-facies to granulite-facies syntaxial rocks today (albeit not necessarily in the past). Most of the white micas in the Bengal Fan were likely derived from Higher Himalayan rocks sourced from outside of the syntaxis. We also note the difference between the multimodal age spectra of the Brahmaputra versus the unimodal population that characterizes the Bengal Fan samples, in which the younger population (i.e., younger than 15 Ma) is absent, even in samples with a depositional age younger than 1 Ma. Gemignani (2018) dated micas from the modern Brahmaputra system and showed that coarser-grained narrow grain-size ranges (e.g., 355–500 and 500–1000 μm) tended to give unimodal peaks, not retaining the younger signal, compared to spectra gained from 125–355 μm grains, which showed multimodal peaks. We sieved at 250 μm, which therefore encompassed both the size range within which one might expect to see the younger signal preserved (125–355 μm), and the coarser interval shown to be unimodal in

the Brahmaputra sediments (e.g., 355–500 and 500–1000 μm). Grain size may therefore explain the lack of a younger signal in the Bengal Fan data. Alternatively, downstream dilution, e.g., due to input from the Ganges and Neogene IBR, may also have caused the lack of retention of the younger part of the spectra. Younger grains do persist >1000 km downstream (Gemignani, 2018), albeit predominantly (although not exclusively) in the finer fraction. Nevertheless, downstream of the analyzed modern Brahmaputra River samples, micas from the Ganges and the Neogene IBR would also contribute to the Bengal Fan signal. The mica age signal of the Neogene IBR rocks is nearly exclusively older than 10 Ma (Najman et al., 2012), and we would expect the Ganges to have a lower proportion of younger grains compared to the Brahmaputra, since the Ganges does not drain the syntaxis.

For the apatite data, since the temperature sensitivity of the U-Pb system in apatite partially overlaps with that of rutile, it might be expected that apatite should yield similar or slightly younger ages compared to rutile from a hypothetical source rock with the same thermal history. However, apatite grains with short (<1 m.y.) lag times were not observed in the Bengal Fan samples or syntaxially derived modern river sediment, in contrast to rutile.

Several possible causes for this difference in U-Pb age pattern can reasonably be eliminated. The absence of syntaxial apatite U-Pb ages is unlikely to be due to source fertility bias or preferential loss of apatite during transport, because most igneous and metamorphic rocks yield apatite (Piccoli and Candela, 2002; Spear and Pyle, 2002), and AFT data are recorded from the syntaxis (e.g., Zeitler et al., 2014), while heavy mineral analysis of modern river sediment of the Ganges-Brahmaputra indicates comparable abundances of rutile and apatite (each phase comprises ~0.7%–1.1% of the heavy mineral fraction), albeit with considerable intersample variability (Garzanti et al., 2010). Small sample sizes are also not likely to be to blame: Although we obtained only limited numbers of acceptable ages, we successfully analyzed ≥ 96 grains per sample (i.e., successful ablations of stoichiometric apatite prior to U-Pb age filtering), similar to rutile. Apatite with low U content (<~1 ppm, typical of low-to medium-grade metapelites and metabasites; Henrichs et al., 2018; O’Sullivan et al., 2018) is also unlikely to be the cause, because the U contents of apatite and rutile analyzed in this study were very similar, as were their radiogenic Pb contents.

However, our apatite data set clearly exhibits higher common Pb content (Pb_c) than rutile (Data Repository Item DR9 [see footnote 1]),

where Pb_c is Pb incorporated during crystallization, and Pb^* is radiogenic Pb generated by in situ U and Th decay. The Pb_c content is significant because the ^{207}Pb -based age correction employed is a projection on Tera-Wasserburg concordia from an assumed $^{207}\text{Pb}/^{206}\text{Pb}$ initial value “through” the analysis to a lower $^{206}\text{Pb}^*/^{238}\text{U}$ intercept, which yields the age. The higher Pb_c/Pb^* in apatite compared to rutile means that young apatite analyses often plot close to the $^{207}\text{Pb}/^{206}\text{Pb}$ intercept on the Tera-Wasserburg concordia, greatly increasing the uncertainty on the lower-intercept age, which means many such grains fail our data-filtering procedure (Section 3.1). Thus, although apatite from the syntaxis is likely present in our samples, especially as the syntaxis is thought to contribute as much as 60%–70% of the modern Brahmaputra sediment load (Enkelmann et al., 2011), we are unable to detect it easily by apatite U-Pb dating due to its elevated Pb_c contents.

Frei et al. (1997) hypothesized that Pb^* is typically tetravalent (due to electron stripping during recoil following α -decay), in contrast to the assumed divalent behavior of Pb_c . Kramers et al. (2009) documented diffusivity of Pb^* in zircon that was 3–4 orders of magnitude lower than that of Pb_c , thus accounting for the extreme retentivity of the zircon U-Pb system at high temperatures because of preferential substitution into the lattice of radiogenic Pb^{4+} for Zr^{4+} . In apatite, the inverse case should apply, with preferential substitution into the lattice of common Pb^{2+} for Ca^{2+} , with radiogenic Pb^{4+} presumably hosted interstitially or in defects. This may account for the elevated Pb_c observed in apatite compared to rutile, because at and above their respective temperature sensitivity windows for Pb-retention, apatite may either more effectively partition matrix (i.e., common) Pb into its crystal lattice, preferentially lose interstitial Pb^* by diffusion, or both.

CONCLUSIONS

The Bengal Fan sedimentary record provides an unparalleled opportunity to record Eastern Himalayan and eastern syntaxial tectonics, allowing, particularly for the latter, remote access to this geographically highly inaccessible area.

Our data provide the first thermochronological study of Bengal Fan material obtained during IODP Expedition 354. We record very short lag times over the period 17–14.5 Ma, and from 3.76–3.47 Ma to <1 Ma. The first occurrence of such short lag times in the younger interval is constrained as beginning no earlier than the youngest analyzed underlying sample recording only long lag times; this sample has a depositional age of 5.59–4.50 Ma.

(1) We interpret the younger period as that of commencement of rapid exhumation in the syntaxial massif, defined as that part of the syntaxial region north of the Nam La Thrust. This data set shows excellent synchronicity with previous work that proposed syntaxis formation occurred as a result of crustal buckling of the constricted corner of the orogen beginning at ca. 3.5 Ma (Burg et al., 1997; Burg and Schmalholz, 2008). Our data are not compatible with previous works that proposed either later or earlier onset of extremely rapid exhumation. Overall, it is clear that our documentation of rapid exhumation starting around ca. 4 Ma is not compatible with models that explain syntaxial evolution either by river capture (Zeitler et al., 2001), which occurred much earlier (Bracciali et al., 2015), or by subduction geometry at indenter corners (Bendick and Ehlers, 2014), which also would require earlier onset.

(2) We interpret the older period of short lag times in our data to reflect the period of rapid exhumation (17–14.5 Ma) of the Greater Himalaya recorded throughout the orogen.

(3) Over the intervening interval from >12 Ma to 5.59–4.50 Ma, rutile and zircon populations show a static lag-time peak, most easily interpreted as passive erosion of the Greater Himalaya following cessation of its period of rapid exhumation as detailed above. However, if single-grain data rather than population data are considered robust, then relatively rapid exhumation is recorded, albeit at a lower rate compared to that recorded above and below this interval. Such grains were most likely sourced from the Greater Himalaya, as detailed above, or for sediments younger than 10 Ma, such grains may alternatively reflect the exhumation of the syntaxial antiform.

(4) While ZFT and rutile U-Pb analyses track syntaxial exhumation very well, the mica $^{40}\text{Ar}/^{39}\text{Ar}$ thermochronometer is better suited to recording exhumation events outside of the syntaxis. Short lag times are only recorded at ca. 16.9 Ma, consistent with the known period of Greater Himalayan exhumation. Our data negate previous proposals that micas with very short lag times are found throughout the Bengal Fan sedimentary record, indicating spatially varied rapid exhumation of the orogen throughout the Neogene.

(5) Likewise, the apatite U-Pb thermochronometer is well suited to recording Himalayan but not syntaxial exhumation. We attribute this to elevated levels of Pb_c in apatite relative to rutile, which lead to poorly constrained ^{207}Pb -corrected U-Pb ages associated with unacceptably high uncertainty. This effect is reduced for older apatite grains, where there has been more time for radiogenic ingrowth, but it is especially

severe in young grains, reflected in the paucity of Neogene–Quaternary apatite U–Pb ages compared to rutile.

ACKNOWLEDGMENTS

Co-chiefs Christian France-Lanord (Centre de Recherches Pétrographiques et Géochimiques—*Centre National de la Recherche Scientifique*), Volkard Spiess (Bremen), and Tilmann Schwenk (Bremen), and Staff Scientist Adam Klaus (International Ocean Discovery Program [IODP]) are acknowledged for initiating, planning, and coordinating IODP Expedition 354. Expedition 354 scientists, IODP staff, and the *Joides* crew are acknowledged for making the expedition a success. Pascale Huyghe is thanked for funding apatite analyses on modern river sands and recent Bengal Fan sediments, and Jacqui Owen is thanked for her contribution to the laboratory work. Devon Orme, an anonymous reviewer, and the associate editor provided critical reviews that improved the quality of this work. This work was funded from Natural Environment Research Council grant NE/N005287/1. Mark and Chew acknowledge support from Science Foundation Ireland under grant number 13/RC/2092, which is co-funded under the European Regional Development Fund and by PIPCO RSG and its member companies. This research used samples and/or data provided by IODP.

REFERENCES CITED

- Adlakha, V., Lang, K.A., Patel, R.C., Lal, N., and Huntington, K.W., 2013, Rapid long-term erosion in the rain shadow of the Shillong Plateau, Eastern Himalaya: *Tectonophysics*, v. 582, p. 76–83, <https://doi.org/10.1016/j.tecto.2012.09.022>.
- Allen, R., Najman, Y., Carter, A., Parrish, R., Bickle, M., Paul, M., Garzanti, E., Reiserberg, L., Chapman, H., Vezzoli, G., and Ando, S., 2008, Provenance of the Tertiary sedimentary rocks of the Indo-Burman Ranges, Burma (Myanmar): Burman arc or Himalayan-derived? *Journal of the Geological Society [London]*, v. 165, p. 1045–1057, <https://doi.org/10.1144/0016-76492007-143>.
- Anczkiewicz, R., Chakraborty, S., Dasgupta, S., Mukhopadhyay, D., and Koltonik, K., 2014, Timing, duration and inversion of prograde Barrovian metamorphism constrained by high resolution Lu–Hf garnet dating: A case study from the Sikkim Himalaya, NE India: *Earth and Planetary Science Letters*, v. 407, p. 70–81, <https://doi.org/10.1016/j.epsl.2014.09.035>.
- Bendick, R., and Ehlers, T.A., 2014, Extreme localized exhumation at syntaxes initiated by subduction geometry: *Geophysical Research Letters*, v. 41, no. 16, p. 5861–5867, <https://doi.org/10.1002/2014GL061026>.
- Bernet, M., van der Beek, P., Pik, R., Huyghe, P., Mugnier, J.L., Labrin, E., and Szulc, A., 2006, Miocene to Recent exhumation of the central Himalaya determined from combined detrital zircon fission-track and U/Pb analysis of Siwalik sediments, western Nepal: *Basin Research*, v. 18, no. 4, p. 393–412, <https://doi.org/10.1111/j.1365-2117.2006.00303.x>.
- Blum, M., Rogers, K., Gleason, J. D., Najman, Y., Cruz, J., and Fox, L., 2018, Allogenic and autogenic signals in the stratigraphic record of the deep-sea Bengal Fan: *Nature Scientific Reports*, v. 8, p. 7973.
- Bollinger, L., and Janots, E., 2006, Evidence for Mio-Pliocene retrograde monazite in the Lesser Himalaya, far western Nepal: *European Journal of Mineralogy*, v. 18, no. 3, p. 289–297, <https://doi.org/10.1127/0935-1221/2006/0018-0289>.
- Booth, A.L., Chamberlain, C.P., Kidd, W.S., and Zeitler, P.K., 2009, Constraints on the metamorphic evolution of the eastern Himalayan syntaxis from geochronologic and petrologic studies of Namche Barwa: *Geological Society of America Bulletin*, v. 121, no. 3–4, p. 385–407, <https://doi.org/10.1130/B26041.1>.
- Bouquillon, A., France-Lanord, C., Michard, A., and Tierce-lin, J., 1990, Sedimentology and isotopic chemistry of the Bengal Fan sediments: The denudation of the Himalaya, in Cochran, J.R., Stow, D.A.V., et al., *Proceedings of the Ocean Drilling Program, Scientific Results, Volume 116: College Station, Texas, Ocean Drilling Program*, p. 43–58.
- Bracciali, L., Parrish, R., Horstwood, M., Condon, D., and Najman, Y., 2013, U–Pb LA-(MC)-ICP-MS dating of rutile: New reference materials and applications to sedimentary provenance: *Chemical Geology*, v. 347, p. 82–101, <https://doi.org/10.1016/j.chemgeo.2013.03.013>.
- Bracciali, L., Najman, Y., Parrish, R.R., Akhter, S.H., and Millar, I., 2015, The Brahmaputra tale of tectonics and erosion: Early Miocene river capture in the Eastern Himalaya: *Earth and Planetary Science Letters*, v. 415, p. 25–37, <https://doi.org/10.1016/j.epsl.2015.01.022>.
- Bracciali, L., Parrish, R.R., Najman, Y., Smye, A., Carter, A., and Wijbrans, J.R., 2016, Plio-Pleistocene exhumation of the eastern Himalayan syntaxis and its domal ‘pop-up’: *Earth-Science Reviews*, v. 160, p. 350–385, <https://doi.org/10.1016/j.earscirev.2016.07.010>.
- Braden, Z., Godin, L., and Cottle, J.M., 2017, Segmentation and rejuvenation of the Greater Himalayan sequence in western Nepal revealed by in situ U–Th/Pb monazite petrochronology: *Lithos*, v. 284–285, p. 751–765, <https://doi.org/10.1016/j.lithos.2017.04.023>.
- Braden, Z., Godin, L., Cottle, J.M., and Yakymchuk, C., 2018, Renewed late Miocene (<8 Ma) hinterland ductile thrusting, western Nepal Himalaya: *Geology*, v. 46, p. 503–506, <https://doi.org/10.1130/G40097.1>.
- Burbank, D., Blythe, A., Putkonen, J., Pratt-Sitaula, B., Gabet, E., Oskin, M., Barros, A., and Ojha, T.P., 2003, Decoupling of erosion and precipitation in the Himalayas: *Nature*, v. 426, p. 652–655, <https://doi.org/10.1038/nature02187>.
- Burg, J.P., and Schmalholz, S.M., 2008, Viscous heating allows thrusting to overcome crustal-scale buckling: Numerical investigation with application to the Himalayan syntaxes: *Earth and Planetary Science Letters*, v. 274, no. 1–2, p. 189–203, <https://doi.org/10.1016/j.epsl.2008.07.022>.
- Burg, J.P., Davy, P., Nievergelt, P., Oberli, F., Seward, D., Diao, Z.Z., and Meier, M., 1997, Exhumation during crustal folding in the Namche-Barwa syntaxis: *Terra Nova*, v. 9, no. 2, p. 53–56, <https://doi.org/10.1111/j.1365-3121.1997.tb00001.x>.
- Burg, J.-P., Nievergelt, P., Oberli, F., Seward, D., Davy, P., Maurin, J.-C., Diao, Z., and Meier, M., 1998, The Namche Barwa syntaxis: Evidence for exhumation related to compressional crustal folding: *Journal of Asian Earth Sciences*, v. 16, no. 2–3, p. 239–252, [https://doi.org/10.1016/S0743-9547\(98\)00002-6](https://doi.org/10.1016/S0743-9547(98)00002-6).
- Carrapa, B., 2010, Resolving tectonic problems by dating detrital minerals: *Geology*, v. 38, no. 2, p. 191–192, <https://doi.org/10.1130/focus022010.1>.
- Carrapa, B., Orme, D.A., DeCelles, P.G., Kapp, P., Cosca, M., and Waldrup, R., 2014, Miocene burial and exhumation of the India-Asia collision zone in southern Tibet: Response to slab dynamics and erosion: *Geology*, v. 42, p. 443–446, <https://doi.org/10.1130/G35350.1>.
- Catlos, E.J., Dubey, C.S., Harrison, T.M., and Edwards, M.A., 2004, Late Miocene movement within the Himalayan Main Central thrust shear zone, Sikkim, north-east India: *Journal of Metamorphic Geology*, v. 22, no. 3, p. 207–226, <https://doi.org/10.1111/j.1525-1314.2004.00509.x>.
- Chew, D., Petrus, J., and Kamber, B., 2014, U–Pb LA-ICPMS dating using accessory mineral standards with variable common Pb: *Chemical Geology*, v. 363, p. 185–199, <https://doi.org/10.1016/j.chemgeo.2013.11.006>.
- Chirouze, F., Huyghe, P., van der Beek, P., Chauvel, C., Chakraborty, T., Dupont-Nivet, G., and Bernet, M., 2013, Tectonics, exhumation, and drainage evolution of the eastern Himalaya since 13 Ma from detrital geochemistry and thermochronology, Kameng River Section, Arunachal Pradesh: *Geological Society of America Bulletin*, v. 125, no. 3–4, p. 523–538, <https://doi.org/10.1130/B30697.1>.
- Cochrane, R., Spikings, R.A., Chew, D., Wotzlaw, J.-F., Chiaradia, M., Tyrrell, S., Schaltegger, U., and Van der Lelij, R., 2014, High temperature (>350 C) thermochronology and mechanisms of Pb loss in apatite: *Geochimica et Cosmochimica Acta*, v. 127, p. 39–56, <https://doi.org/10.1016/j.gca.2013.11.028>.
- Copeland, P., and Harrison, T.M., 1990, Episodic rapid uplift in the Himalaya revealed by Ar-40/Ar-39 analysis of detrital K-feldspar and muscovite, Bengal Fan: *Geology*, v. 18, no. 4, p. 354–357, [https://doi.org/10.1130/0091-7613\(1990\)018<0354:ERUITH>2.3.CO;2](https://doi.org/10.1130/0091-7613(1990)018<0354:ERUITH>2.3.CO;2).
- Corrigan, J.D., and Crowley, K.D., 1990, Fission-track analysis of detrital apatites from sites 717 and 718, leg 116, central Indian Ocean, in Cochran, J.R., Stow, D.A.V., et al., *Proceedings of the Ocean Drilling Program, Scientific Results, Volume 116: College Station, Texas, Ocean Drilling Program*, p. 75–83.
- Cottle, J.M., Searle, M.P., Horstwood, M.S.A., and Waters, D.J., 2009, timing of midcrustal metamorphism, melting, and deformation in the Mount Everest region of southern Tibet revealed by U-(Th)-Pb geochronology: *The Journal of Geology*, v. 117, no. 6, p. 643–664, <https://doi.org/10.1086/605994>.
- Coutand, I., Whipp, D.M., Grujic, D., Bernet, M., Fellin, M.G., Bookhagen, B., Landry, K.R., Ghalley, S.K., and Duncan, C., 2014, Geometry and kinematics of the Main Himalayan thrust and Neogene crustal exhumation in the Bhutanese Himalaya derived from inversion of multithermochronologic data: *Journal of Geophysical Research—Solid Earth*, v. 119, no. 2, p. 1446–1481, <https://doi.org/10.1002/2013JB010891>.
- Ding, L., Zhong, D., Yin, A., Kapp, P., and Harrison, T.M., 2001, Cenozoic structural and metamorphic evolution of the eastern Himalayan syntaxis (Namche Barwa): *Earth and Planetary Science Letters*, v. 192, no. 3, p. 423–438, [https://doi.org/10.1016/S0012-821X\(01\)00463-0](https://doi.org/10.1016/S0012-821X(01)00463-0).
- Enkelmann, E., Ehlers, T.A., Zeitler, P.K., and Hallet, B., 2011, Denudation of the Namche Barwa antiform, eastern Himalaya: *Earth and Planetary Science Letters*, v. 307, no. 3–4, p. 323–333, <https://doi.org/10.1016/j.epsl.2011.05.004>.
- Ferry, J. M., and Watson, E.B., 2007, New thermodynamic models and revised calibrations for the Ti-in-zircon and Zr-in-rutile thermometers: Contributions to Mineralogy and Petrology, v. 154, p. 429–437, <https://doi.org/10.1007/s00410-007-0201-0>.
- France-Lanord, C., Spiess, V., Klaus, A., Schwenk, T., and the Expedition 354 Scientists, 2016, Bengal Fan: College Station, Texas, *Proceedings of the International Ocean Discovery Program, 354*, <http://dx.doi.org/10.14379/iodp.proc.354.2016>.
- Frei, R., Villa, I.M., Nägler, T.F., Kramers, J.D., Przybyłowicz, W., Prozesky, V., Hofmann, B., and Kamber, B., 1997, Single mineral dating by the PbPb step-leaching method: Assessing the mechanisms: *Geochimica et Cosmochimica Acta*, v. 61, no. 2, p. 393–414, [https://doi.org/10.1016/S0016-7037\(96\)00343-2](https://doi.org/10.1016/S0016-7037(96)00343-2).
- Galbraith, R.F., 2005, *Statistics for Fission Track Analysis: Chapman and Hall/CRC, Interdisciplinary Statistics Series*, 224 p.
- Garzanti, E., Andò, S., France-Lanord, C., Vezzoli, G., Censi, P., Galy, V., and Najman, Y., 2010, Mineralogical and chemical variability of fluvial sediments: 1. Bedload sand (Ganga–Brahmaputra, Bangladesh): *Earth and Planetary Science Letters*, v. 299, no. 3, p. 368–381, <https://doi.org/10.1016/j.epsl.2010.09.017>.
- Ge, Y., Li, Y., Wang, X., Zhang, J., Zhou, A., and Liu-Zeng, J., 2018, Oligocene–Miocene burial and exhumation of the southernmost Gangdese mountains from sedimentary and thermochronological data: *Tectonophysics*, v. 723, p. 68–80, <https://doi.org/10.1016/j.tecto.2017.12.003>.
- Gemignani, L., 2018, *Extracting Erosion and Exhumation Patterns from Detrital Thermochronology: An Example from the Eastern Himalaya [Ph.D. thesis]: Amsterdam, Netherlands, Vrije Universiteit*, 185 p.
- Gemignani, L., Van der Beek, P., Braun, J., Najman, Y., Bernet, Y., Garzanti, E., and Wijbrans, J.R., 2018, Downstream evolution of the thermochronologic age signal in the Brahmaputra catchment: Implications for erosion of the Eastern Himalaya: *Earth and Planetary Science Letters*, v. 499, p. 48–61, <https://doi.org/10.1016/j.epsl.2018.07.019>.

- Godin, L., Parrish, R.R., Brown, R.L., and Hodges, K.V., 2001, Crustal thickening leading to exhumation of the Himalayan metamorphic core of central Nepal: Insight from U-Pb geochronology and Ar-40/Ar-39 thermochronology: *Tectonics*, v. 20, no. 5, p. 729–747, <https://doi.org/10.1029/2000TC001204>.
- Godin, L., Grujic, D., Law, R.D., and Searle, M.P., 2006, Channel flow, ductile extrusion and exhumation in continental collision zones: An introduction, in Law, R.D., Searle, M.P., and Godin, L., eds., *Channel Flow, Ductile Extrusion and Exhumation in Continental Collision Zones*: Geological Society [London] Special Publication 268, p. 1–23.
- Govin, G., 2017, Tectonic-Erosion Interactions: Insights from the Palaeo-Drainage of the Brahmaputra River [Ph.D. thesis]: Lancaster, UK, Lancaster University, 331 p.
- Govin, G., Van der Beek, P., Najman, Y., Millar, I., Bernert, M., Gemignani, L., Huyghe, P., Wijbrans, J., and Dupont-Nivet, G., 2017, Onset of rapid exhumation in the Namche Barwa syntaxis constrained by detrital thermochronology: New Orleans, Louisiana, American Geophysical Union, Fall Meeting 2017, abstract T12A-04.
- Guilmette, C., Indares, A., and Hébert, R., 2011, High-pressure anatexis paragneisses from the Namche Barwa, eastern Himalayan syntaxis: Textural evidence for partial melting, phase equilibria modeling and tectonic implications: *Lithos*, v. 124, no. 1, p. 66–81, <https://doi.org/10.1016/j.lithos.2010.09.003>.
- Harrison, T.M., Celerier, J., Aikman, A.B., Hermann, J., and Heizler, M.T., 2009, Diffusion of 40-Ar in muscovite: *Geochimica et Cosmochimica Acta*, v. 73, p. 1039–1051, <https://doi.org/10.1016/j.gca.2008.09.038>.
- Henrichs, I., O'Sullivan, G., Chew, D.M., Mark, C., Babechuk, M.G., McKenna, C., and Emo, R., 2018, The trace element and U-Pb systematics of metamorphic apatite: *Chemical Geology*, v. 483, p. 218–238, <https://doi.org/10.1016/j.chemgeo.2017.12.031>.
- Hodges, K.V., 2000, Tectonics of the Himalaya and southern Tibet from two perspectives: *Geological Society of America Bulletin*, v. 112, no. 3, p. 324–350, [https://doi.org/10.1130/0016-7606\(2000\)112<324:TOTHAS>2.0.CO;2](https://doi.org/10.1130/0016-7606(2000)112<324:TOTHAS>2.0.CO;2).
- Hu, X., Garzanti, E., Wang, J., Huang, W., An, W., and Webb, A., 2016, The timing of India-Asia collision onset—Facts, theories, controversies: *Earth-Science Reviews*, v. 160, p. 264–299, <https://doi.org/10.1016/j.earscirev.2016.07.014>.
- Hubbard, M.S., and Harrison, T.M., 1989, Ar-40/Ar-39 age constraints on deformation and metamorphism in the Main Central thrust zone and Tibetan slab, eastern Nepal Himalaya: *Tectonics*, v. 8, no. 4, p. 865–880, <https://doi.org/10.1029/TC008i004p0865>.
- Hurford, A.J., 1990, Standardization of fission track dating calibration: Recommendation by the Fission Track Working Group of the IUGS Subcommittee on Geochronology: *Chemical Geology*, v. 80, p. 177–178.
- Johnson, S.Y., and Alam, A.M.N., 1991, Sedimentation and tectonics of the Sylhet Trough, Bangladesh: *Geological Society of America Bulletin*, v. 103, no. 11, p. 1513–1527, [https://doi.org/10.1130/0016-7606\(1991\)103<1513:SATOTS>2.3.CO;2](https://doi.org/10.1130/0016-7606(1991)103<1513:SATOTS>2.3.CO;2).
- Kellett, D.A., Grujic, D., Coutand, I., Cottle, J., and Mukul, M., 2013, The South Tibetan detachment system facilitates ultra rapid cooling of granulite-facies rocks in Sikkim Himalaya: *Tectonics*, v. 32, no. 2, p. 252–270, <https://doi.org/10.1002/tect.20014>.
- King, G.E., Herman, F., and Guralnik, B., 2016, Northward migration of the eastern Himalayan syntaxis revealed by OSL thermochronometry: *Science*, v. 353, no. 6301, p. 800–804, <https://doi.org/10.1126/science.aaf2637>.
- Kooijman, E., Mezger, K., and Berndt, J., 2010, Constraints on the U-Pb systematics of metamorphic rutile from in situ LA-ICP-MS analysis: *Earth and Planetary Science Letters*, v. 293, no. 3, p. 321–330, <https://doi.org/10.1016/j.epsl.2010.02.047>.
- Kramers, J., Frei, R., Newville, M., Kober, B., and Villa, I., 2009, On the valency state of radiogenic lead in zircon and its consequences: *Chemical Geology*, v. 261, no. 1, p. 4–11, <https://doi.org/10.1016/j.chemgeo.2008.09.010>.
- Lang, K.A., Huntington, K.W., Burmester, R., and Housen, B., 2016, Rapid exhumation of the eastern Himalayan syntaxis since the late Miocene: *Geological Society of America Bulletin*, v. 128, no. 9–10, p. 1403–1422, <https://doi.org/10.1130/B31419.31411>.
- Larson, K.P., Camacho, A., Cottle, J.M., Coutand, I., Buckingham, H.M., Ambrose, T.K., and Rai, S.M., 2017, Cooling, exhumation, and kinematics of the Kanchenjunga Himal, far east Nepal: *Tectonics*, v. 36, no. 6, p. 1037–1052, <https://doi.org/10.1002/2017TC004496>.
- Leary, R.J., DeCelles, P., Quade, J., Gehrels, G., and Waanders, G., 2016, The Liuku conglomerate, southern Tibet: Early Miocene basin development related to deformation within the Great Counter Thrust system: *Lithosphere*, v. 8, p. 427–450, <https://doi.org/10.1130/L542.1>.
- Liu, Y., Siebel, W., Theye, T., and Massonne, H.-J., 2011, Isotopic and structural constraints on the late Miocene to Pliocene evolution of the Namche Barwa area, eastern Himalayan syntaxis, SE Tibet: *Gondwana Research*, v. 19, p. 894–909, <https://doi.org/10.1016/j.gr.2010.11.005>.
- Ludwig, K., 2012, User's Manual for Isoplot 3.75: A Geochronological Toolkit for Microsoft Excel: Berkeley Geochronology Center Special Publication 5, 75 p.
- Luvizotto, G., Zack, T., Meyer, H., Ludwig, T., Triebold, S., Krontz, A., Munker, C., Stockli, D., Prowatke, S., and Klemme, S., 2009, Rutile crystals as potential trace element and isotope mineral standards for microanalysis: *Chemical Geology*, v. 261, no. 3, p. 346–369, <https://doi.org/10.1016/j.chemgeo.2008.04.012>.
- Malusà, M. G., Resentini, A., and Garzanti, E., 2016, Hydraulic sorting and mineral fertility bias in detrital geochronology: *Gondwana Research*, v. 31, Supplement C, p. 1–19, <https://doi.org/10.1016/j.gr.2015.09.002>.
- Mark, C., Cogné, N., and Chew, D., 2016, Tracking exhumation and drainage divide migration of the western Alps: A test of the apatite U-Pb thermochronometer as a detrital provenance tool: *Geological Society of America Bulletin*, v. 128, no. 9–10, p. 1439–1460, <https://doi.org/10.1130/B31351.1>.
- Maurin, T., and Rangin, C., 2009, Structure and kinematics of the Indo-Burmese eedge: Recent and fast growth of the outer wedge: *Tectonics*, v. 28, TC2010, <https://doi.org/10.1029/2008TC002276>.
- McDougall, I., and Harrison, T.M., 1999, *Geochronology and Thermochronology by the ⁴⁰Ar/³⁹Ar Method*: Oxford, UK, Oxford University Press, 269 p.
- McDowell, F.W., McIntosh, W.C., and Farley, K.A., 2005, A precise ⁴⁰Ar-³⁹Ar reference age for the Durango apatite (U-Th)/He and fission-track dating standard: *Chemical Geology*, v. 214, no. 3, p. 249–263, <https://doi.org/10.1016/j.chemgeo.2004.10.002>.
- McNeill, L.C., Dugan, B., Backman, J., Pickering, K.T., Poudouret, H.F.A., Henstock, T.J., Petronotis, K.E., Carter, A., Chemale, F., Milliken, K.L., Kutterolf, S., Mukoyoshi, H., Chen, W.H., Kachovich, S., Mitchison, F.L., Bourlange, S., Colson, T.A., Frederik, M.C.G., Guerin, G., Hamahashi, M., House, B.M., Hupers, A., Jeppson, T.N., Kenigsberg, A.R., Kuranaga, M., Nair, N., Owari, S., Shan, Y.H., Song, I.S., Torres, M.E., Vannucchi, P., Vrolijk, P.J., Yang, T., Zhao, X.X., and Thomas, E., 2017, Understanding Himalayan erosion and the significance of the Nicobar Fan: *Earth and Planetary Science Letters*, v. 475, p. 134–142, <https://doi.org/10.1016/j.epsl.2017.07.019>.
- Meinhold, G., 2010, Rutile and its applications in earth sciences: *Earth-Science Reviews*, v. 102, p. 1–28, <https://doi.org/10.1016/j.earscirev.2010.06.001>.
- Mottram, C.M., Parrish, R.R., Regis, D., Warren, C.J., Argles, T.W., Harris, N.B.W., and Roberts, N.M.W., 2015, Using U-Th-Pb petrochronology to determine rates of ductile thrusting: Time windows into the Main Central thrust, Sikkim Himalaya: *Tectonics*, v. 34, no. 7, p. 1355–1374, <https://doi.org/10.1002/2014TC003743>.
- Mottram, C.M., Warren, C.J., Regis, D., Roberts, N.M.W., Harris, N.B.W., Argles, T.W., and Parrish, R.R., 2014, Developing an inverted Barrovian sequence: insights from monazite petrochronology: *Earth and Planetary Science Letters*, v. 403, p. 418–431, <https://doi.org/10.1016/j.epsl.2014.07.006>.
- Najman, Y., Bickle, M., BouDagher-Fadel, M., Carter, A., Garzanti, E., Paul, M., Wijbrans, J., Willett, E.,
- Oliver, G., Parrish, R., Akhter, S.H., Allen, R., Ando, S., Chisty, E., Reisberg, L., and Vezzoli, G., 2008, The Paleogene record of Himalayan erosion: Bengal Basin, Bangladesh: *Earth and Planetary Science Letters*, v. 273, no. 1–2, p. 1–14, <https://doi.org/10.1016/j.epsl.2008.04.028>.
- Najman, Y., Bickle, M., Garzanti, E., Pringle, M., Barford, D., Brozovic, N., Burbank, D., and Ando, S., 2009, Reconstructing the exhumation history of the Lesser Himalaya, NW India, from a multitechnique provenance study of the foreland basin Siwalik Group: *Tectonics*, v. 28, TC5018, <https://doi.org/10.1029/2009TC002506>.
- Najman, Y., Allen, R., Willett, E.A.F., Carter, A., Barford, D., Garzanti, E., Wijbrans, J., Bickle, M., Vezzoli, G., Ando, S., Oliver, G., and Uddin, M., 2012, The record of Himalayan erosion preserved in the sedimentary rocks of the Hatia Trough of the Bengal Basin and the Chittagong Hill Tracts, Bangladesh: *Basin Research*, v. 24, p. 499–519, <https://doi.org/10.1111/j.1365-2117.2011.00540.x>.
- Najman, Y., Bracciali, L., Parrish, R.R., Chisty, E., and Copley, A., 2016, Evolving strain partitioning in the Eastern Himalaya: The growth of the Shillong Plateau: *Earth and Planetary Science Letters*, v. 433, p. 1–9, <https://doi.org/10.1016/j.epsl.2015.10.017>.
- Najman, Y., Jenks, D., Godin, L., Boudagher-Fadel, M., Millar, I., Garzanti, E., Horstwood, M., and Bracciali, L., 2017, The Tethyan Himalayan detrital record shows that India-Asia terminal collision occurred by 54 Ma in the Western Himalaya: *Earth and Planetary Science Letters*, v. 459, p. 301–310, <https://doi.org/10.1016/j.epsl.2016.11.036>.
- O'Sullivan, G.J., Chew, D.M., and Samson, S.D., 2016, Detecting magma-poor orogens in the detrital record: *Geology*, v. 44, no. 10, p. 871–874, <https://doi.org/10.1130/G38245.1>.
- O'Sullivan, G., Chew, D. M., Morton, A., Mark, C., and Henrichs, I., 2018, An integrated apatite geochronology and geochemistry tool for sedimentary provenance analysis: *Geochemistry Geophysics Geosystems*, v. 19, p. 1309–1326, <https://doi.org/10.1002/2017GC007343>.
- Palin, R.M., Searle, M.P., St-Onge, M.R., Waters, D.J., Roberts, N.M.W., Horstwood, M.S.A., Parrish, R.R., and Weller, O.M., 2015, Two-stage cooling history of pelitic and semi-pelitic mylonite (sensu lato) from the Dongjiu-Milin shear zone, northwest flank of the eastern Himalayan syntaxis: *Gondwana Research*, v. 28, no. 2, p. 509–530, <https://doi.org/10.1016/j.gr.2014.07.009>.
- Paton, C., Hellstrom, J., Paul, B., Woodhead, J., and Hergt, J., 2011, Iolite: Freeware for the visualisation and processing of mass spectrometric data: *Journal of Analytical Atomic Spectrometry*, v. 26, no. 12, p. 2508–2518, <https://doi.org/10.1039/c1ja10172b>.
- Piccoli, P.M., and Candela, P.A., 2002, Apatite in igneous systems: Reviews in Mineralogy and Geochemistry, v. 48, no. 1, p. 255–292, <https://doi.org/10.2138/rmg.2002.48.6>.
- Rahn, M., Brandon, M.T., Batt, G., and Garver, J.I., 2004, A zero-damage model for fission-track annealing in zircon: *The American Mineralogist*, v. 89, p. 473–484, <https://doi.org/10.2138/am-2004-0401>.
- Renne, P.R., Balco, G., Ludwig, K.R., Mundil, R., and Min, K., 2011, Response to the comment by W.H. Schwarz et al. on "Joint determination of ⁴⁰K decay constants and ⁴⁰Ar/³⁹K for the Fish Canyon sanidine standard, and improved accuracy for ⁴⁰Ar/³⁹Ar geochronology" by P.R. Renne et al. (2010): *Geochimica et Cosmochimica Acta*, v. 75, no. 17, p. 5097, <https://doi.org/10.1016/j.gca.2011.06.021>.
- Schoene, B., and Bowring, S.A., 2006, U-Pb systematics of the McClure Mountain syenite: Thermochronological constraints on the age of the ⁴⁰Ar/³⁹Ar standard MMhb: *Contributions to Mineralogy and Petrology*, v. 151, no. 5, p. 615, <https://doi.org/10.1007/s00410-006-0077-4>.
- Searle, M.P., Cottle, J.M., Streule, M.J., and Waters, D.J., 2009, Crustal melt granites and migmatites along the Himalaya: Melt source, segregation, transport and granite emplacement mechanisms: *Earth and Environmental Science Transactions of the Royal Society of Edinburgh*, v. 100, no. 1–2, p. 219–233, <https://doi.org/10.1017/S175569100901617X>.

- Seward, D., and Burg, J.-P., 2008, Growth of the Namche Barwa syntaxis and associated evolution of the Tsangpo Gorge: Constraints from structural and thermochronological data: *Tectonophysics*, v. 451, no. 1–4, p. 282–289, <https://doi.org/10.1016/j.tecto.2007.11.057>.
- Shi, G., Li, X., Li, Q., Chen, Z., Deng, J., Liu, Y., Kang, Z., Pang, E., Xu, Y., and Jia, X., 2012, Ion microprobe U-Pb age and Zr-in-rutile thermometry of rutiles from the Daixian rutile deposit in the Hengshan Mountains, Shanxi Province, China: *Economic Geology and the Bulletin of the Society of Economic Geologists*, v. 107, no. 3, p. 525–535, <https://doi.org/10.2113/econgeo.107.3.525>.
- Simpson, R.L., Parrish, R.R., Searle, M.P., and Waters, D.J., 2000, Two episodes of monazite crystallization during metamorphism and crustal melting in the Everest region of the Nepalese Himalaya: *Geology*, v. 28, no. 5, p. 403–406, [https://doi.org/10.1130/0091-7613\(2000\)28<403:TEOMCD>2.0.CO;2](https://doi.org/10.1130/0091-7613(2000)28<403:TEOMCD>2.0.CO;2).
- Spear, F.S., and Pyle, J.M., 2002, Apatite, monazite, and xenotime in metamorphic rocks: Reviews in Mineralogy and Geochemistry, v. 48, no. 1, p. 293–335, <https://doi.org/10.2138/rmg.2002.48.7>.
- Stacey, J.T., and Kramers, J., 1975, Approximation of terrestrial lead isotope evolution by a two-stage model: *Earth and Planetary Science Letters*, v. 26, no. 2, p. 207–221, [https://doi.org/10.1016/0012-821X\(75\)90088-6](https://doi.org/10.1016/0012-821X(75)90088-6).
- Szulec, A.G., Najman, Y., Sinclair, H.D., Pringle, M., Bickle, M., Chapman, H., Garzanti, E., Ando, S., Huyghe, P., Mugnier, J.L., Ojha, T., and DeCelles, P.G., 2006, Tectonic evolution of the Himalaya constrained by detrital ^{40}Ar - ^{39}Ar , Sm-Nd and petrographic data from the Siwalik foreland basin succession, SW Nepal: *Basin Research*, v. 18, no. 4, p. 375–391, <https://doi.org/10.1111/j.1365-2117.2006.00307.x>.
- Thiede, R.C., and Ehlers, T.A., 2013, Large spatial and temporal variations in Himalayan denudation: *Earth and Planetary Science Letters*, v. 371, p. 278–293, <https://doi.org/10.1016/j.epsl.2013.03.004>.
- Thomson, S.N., Gehrels, G.E., Ruiz, J., and Buchwaldt, R., 2012, Routine low-damage apatite U-Pb dating using laser ablation-multicollector-ICPMS: *Geochemistry Geophysics Geosystems*, v. 13, no. 2, Q0AA21, <https://doi.org/10.1029/2011GC003928>.
- Tomkins, H., Powell, R., and Ellis, D., 2007, The pressure dependence of the zirconium-in-rutile thermometer: *Journal of Metamorphic Geology*, v. 25, no. 6, p. 703–713, <https://doi.org/10.1111/j.1525-1314.2007.00724.x>.
- Tremblay, M.M., Fox, M., Schmidt, J.L., Tripathy-Lang, A., Wielicki, M.M., Harrison, T.M., Zeitler, P.K., and Shuster, D.L., 2015, Erosion in southern Tibet shut down at ~10 Ma due to enhanced rock uplift within the Himalaya: *PNAS*, v. 112, p. 12030–12035, <https://doi.org/10.1073/pnas.1515652112>.
- Turab, S.A., Stuwe, K., Stuart, F.M., Chew, D.M., and Cogne, N., 2017, Tectonics drives rapid exhumation of the western Himalayan syntaxis: Evidence from low-temperature thermochronometry of the Neelum valley region, Pakistan: *Lithosphere*, v. 9, p. 874–888, <https://doi.org/10.1130/L626.1>.
- Vannay, J.C., and Hodges, K.V., 1996, Tectonometamorphic evolution of the Himalayan metamorphic core between Annapurna and Dhaulagiri, central Nepal: *Journal of Metamorphic Geology*, v. 14, no. 5, p. 635–656, <https://doi.org/10.1046/j.1525-1314.1996.00426.x>.
- Vannay, J.C., Grasemann, B., Rahn, M., Frank, W., Carter, A., Baudraz, V., and Cosca, M., 2004, Miocene to Holocene exhumation of metamorphic crustal wedges in the NW Himalaya: Evidence for tectonic extrusion coupled to fluvial erosion: *Tectonics*, v. 23, TC1014, <https://doi.org/10.1029/2002TC001429>.
- Vermeesch, P., 2012, On the visualisation of detrital age distributions: *Chemical Geology*, v. 312, p. 190–194, <https://doi.org/10.1016/j.chemgeo.2012.04.021>.
- Wang, P., Scherler, D., Jing, L.Z., Mey, J., Avouac, J.P., Zhang, Y.D., and Shi, D.G., 2014, Tectonic control of Yarlung Tsangpo Gorge revealed by a buried canyon in southern Tibet: *Science*, v. 346, no. 6212, p. 978–981, <https://doi.org/10.1126/science.1259041>.
- Wang, P., Scherler, D., Jing, L.Z., Mey, J., Avouac, J.P., Zhang, Y.D., and Shi, D.G., 2015, Response to Comment on “Tectonic control of Yarlung Tsangpo Gorge revealed by a buried canyon in southern Tibet”: *Science*, v. 349, no. 6250, p. 799, <https://doi.org/10.1126/science.aaa9636>.
- Whipp, D.M., Beaumont, C., and Braun, J., 2014, Feeding the “aneurysm”: Orogen-parallel mass transport into Nanga Parbat and the western Himalayan syntaxis: *Journal of Geophysical Research—Solid Earth*, v. 119, no. 6, p. 5077–5096, <https://doi.org/10.1002/2013JB010929>.
- White, N.M., Pringle, M., Garzanti, E., Bickle, M., Najman, Y., Chapman, H., and Friend, P., 2002, Constraints on the exhumation and erosion of the High Himalayan slab, NW India, from foreland basin deposits: *Earth and Planetary Science Letters*, v. 195, no. 1–2, p. 29–44, [https://doi.org/10.1016/S0012-821X\(01\)00565-9](https://doi.org/10.1016/S0012-821X(01)00565-9).
- Woodhead, J.D., Hellstrom, J., Hergt, J.M., Greig, A., and Maas, R., 2007, Isotopic and elemental imaging of geological materials by laser ablation inductively coupled plasma-mass spectrometry: *Geostandards and Geoanalytical Research*, v. 31, no. 4, p. 331–343.
- Xia, X., Ren, Z., Wei, G., Zhang, L., Sun, M., and Wang, Y., 2013, In situ rutile U-Pb dating by laser ablation-MC-ICPMS: *Geochemical Journal*, v. 47, p. 459–468, <https://doi.org/10.2343/geochemj.2.0267>.
- Xu, W.-C., Zhang, H.-F., Parrish, R., Harris, N., Guo, L., and Yuan, H.-L., 2010, Timing of granulite-facies metamorphism in the eastern Himalayan syntaxis and its tectonic implications: *Tectonophysics*, v. 485, no. 1, p. 231–244, <https://doi.org/10.1016/j.tecto.2009.12.023>.
- Yang, R., Herman, F., Fellin, M.G., and Maden, C., 2018, Exhumation and topographic evolution of the Namche Barwa syntaxis, Eastern Himalaya: *Tectonophysics*, v. 722, p. 43–52, <https://doi.org/10.1016/j.tecto.2017.10.026>.
- Yin, A., Dubey, C.S., Kelty, T.K., Webb, A.A.G., Harrison, T.M., Chou, C.Y., and Celerier, J., 2010, Geologic correlation of the Himalayan orogen and Indian craton: Part 2. Structural geology, geochronology, and tectonic evolution of the Eastern Himalaya: *Geological Society of America Bulletin*, v. 122, no. 3–4, p. 360–395, <https://doi.org/10.1130/B26461.1>.
- Zack, T., Moraes, R., and Kronz, A., 2004, Temperature dependence of Zr in rutile: Empirical calibration of a rutile thermometer: *Contributions to Mineralogy and Petrology*, v. 148, no. 4, p. 471–488, <https://doi.org/10.1007/s00410-004-0617-8>.
- Zattin, M., Andreucci, B., Thomson, S.N., Reiners, P.W., and Talarico, F.M., 2012, New constraints on the provenance of the ANDRILL AND-2A succession (western Ross Sea, Antarctica) from apatite triple dating: *Geochemistry Geophysics Geosystems*, v. 13, no. 10, Q10016, <https://doi.org/10.1029/2012GC004357>.
- Zeh, A., 2004, Crystal size distribution (CSD) and textural evolution of accessory apatite, titanite and allanite during four stages of metamorphism: An example from the Moine Supergroup, Scotland: *Journal of Petrology*, v. 45, no. 10, p. 2101–2132, <https://doi.org/10.1093/ptrology/egh049>.
- Zeitler, P.K., Meltzer, A.S., Koons, P.O., Craw, D., Hallet, B., Chamberlain, C.P., Kidd, W.S.F., Park, S.K., Seebert, L., Bishop, M., and Shroder, J., 2001, Erosion, Himalayan geodynamics and the geomorphology of metamorphism: *GSA Today*, v. 11, no. 1, p. 4–9.
- Zeitler, P.K., Meltzer, A.S., Brown, L., Kidd, W.S.F., Lim, C., and Enkelmann, E., 2014, Tectonics and topographic evolution of Namche Barwa and the easternmost Lhasa Block, *in* Nie, J., Hoke, G.D., and Horton, B., eds., *Towards an Improved Understanding of Uplift Mechanisms and Elevation History of the Tibetan Plateau*: *Geological Society of America Special Paper* 507, p. 23–58, [https://doi.org/10.1130/2014.2507\(02\)](https://doi.org/10.1130/2014.2507(02)).
- Zeitler, P.K., Koons, P.O., Hallet, B., and Meltzer, A.S., 2015, Comment on “Tectonic control of Yarlung Tsangpo Gorge revealed by a buried canyon in southern Tibet”: *Science*, v. 349, no. 6250, p. 799, <https://doi.org/10.1126/science.aaa9380>.
- Zhang, Z.M., Zhao, G.C., Santosh, M., Wang, J.L., Dong, X., and Liou, J.G., 2010, Two stages of granulite facies metamorphism in the eastern Himalayan syntaxis, south Tibet: Petrology, zircon geochronology and implications for the subduction of Neo-Tethys and the Indian continent beneath Asia: *Journal of Metamorphic Geology*, v. 28, no. 7, p. 719–733, <https://doi.org/10.1111/j.1525-1314.2010.00885.x>.

SCIENCE EDITOR: BRAD SINGER
ASSOCIATE EDITOR: BARBARA CARRAPA

MANUSCRIPT RECEIVED 28 APRIL 2018
REVISED MANUSCRIPT RECEIVED 25 AUGUST 2018
MANUSCRIPT ACCEPTED 29 JANUARY 2019

Printed in the USA